

pubs.acs.org/EF Review

Inverse Oxide/Metal Catalysts for CO₂ Hydrogenation to Methanol

Kashala Fabrice Kapiamba, [∇] Hope O. Otor, [∇] Sridhar Viamajala, and Ana C. Alba-Rubio*



Cite This: Energy Fuels 2022, 36, 11691-11711



ACCESS |

III Metrics & More

Article Recommendations

ABSTRACT: The hydrogenation of CO₂ to methanol using heterogeneous catalysts is an appealing route for mitigating greenhouse gas emissions and generating useful products. The synthesis of methanol is attractive due to its utilization as a fuel, a fuel additive, or an intermediate for a wide array of industrial chemicals. Traditional catalytic systems, like those based on Cu or Ni, have been extensively explored but have thus far shown limited conversion and selectivity to desired products like methanol primarily due to the chemical stability of CO₂. These catalysts are also difficult to use industrially due to the high pressures and temperatures needed for these catalytic reactions. In the search for improvements in the reaction rates, conversion, and selectivity to liquid products, inverse oxide/metal catalysts have been recently



explored and have yielded promising results. This review summarizes the latest advances in the use of inverse catalysts for the hydrogenation of CO₂ to methanol. First, this review focuses on some strategies for synthesizing inverse oxide/metal catalysts. Next, the relationship between the interfacial properties and the catalytic activity is reviewed, emphasizing the nature of the oxide layer and its dispersion on the metal surface. Lastly, the activities of inverse catalysts and materials prepared by traditional synthesis approaches are compared.

1. INTRODUCTION

The atmospheric concentration of carbon dioxide, which has been on the rise since the first industrial revolution, leads to adverse effects on the planet, including climate change and ocean acidification.^{1,2} The majority of CO₂ emissions are energy-related, with transportation, electricity, and heating accounting for two-thirds of the global emissions.³ In the US, CO₂ emissions from energy systems are projected to increase by an average of 3% from 2013 to 2040. Some recent CO₂ mitigation approaches have been focused on CO2 capture and conversion into value-added products, such as hydrocarbons and alcohols. 1,4-7 However, due to the high stability of the CO₂ molecule, its transformation is challenging but potentially feasible if highly active catalysts are used. To achieve effective CO₂ transformation, both thermal and electrocatalytic methods using different transition and precious metal catalysts have been investigated. 5,9-11 Some of the reactions for CO₂ hydrogenation include the reverse water-gas shift (RWGS) reaction (eq 1), CO₂ methanation (eq 2), and CO₂ conversion to alcohols, mainly methanol, either directly (eq 3) or via a CO intermediate (eq 4).

$$CO_2 + H_2 \leftrightharpoons CO + H_2O;$$
 $\Delta H_r^{\circ} = +41.2 \text{ kJ mol}^{-1}$ (1)

$$CO_2 + 4H_2 = CH_4 + 2H_2O;$$

 $\Delta H_r^{\circ} = -165.0 \text{ kJ mol}^{-1}$ (2)

$$CO_2 + 3H_2 \leftrightharpoons CH_3OH + H_2O;$$

$$\Delta H_{\rm r}^{\rm o} = -49.4 \text{ kJ mol}^{-1}$$
 (3)

$$CO + 2H_2 \leftrightharpoons CH_3OH; \quad \Delta H_r^{\circ} = -90.4 \text{ kJ mol}^{-1}$$
 (4

In addition to alcohols, the CO intermediate from the RWGS reaction can also potentially be converted to higher hydrocarbons and liquid products, such as diesel and gasoline, via the Fischer–Tropsch process $((2n+1)H_2 + nCO \rightarrow C_nH_{2n+2} + nH_2O)$.

While the RWGS reaction mainly involves the use of Cu-, Pt-, and Rh-based catalysts, the methanation reaction (eq 2), also referred to as the Sabatier reaction, has been mainly studied using supported Ni, Ru, Rh, and Pd catalysts. 12-15 Although the methanation reaction is thermodynamically

Received: June 27, 2022 Revised: August 27, 2022 Published: September 9, 2022





favorable ($\Delta G_{298K} = -130.8 \text{ kJ/mol}$), the reduction of fully oxidized carbon to methane involves four-electron pairs, making the reaction kinetically limited. Stoichiometrically, this reaction also consumes the most hydrogen, imposing a significant expense on the process. In addition, the reaction is structure-sensitive; hence special attention is needed for preparing suitable catalysts. Although Ni is the most widely studied metal for the methanation reaction, Ru, which is rare and expensive, has been reported to be more active than Ni. As a result, Ru and Ni have also been widely used to develop dual-functional materials (DFMs) for CO_2 capture and conversion to CH_4 . To

The CO₂-to-methanol (CTM) reaction (eq 3) has also gained much research interest due to the ease of storage and transportation of methanol compared to methane, as well as the use of methanol as a commodity chemical and precursor of other compounds, such as formaldehyde and methyl *tert*-butyl ether (MTBE), among others. ^{18–21} Most of the catalysts used for CTM are composed of Cu and ZnO with the addition of modifiers or promoters, such as ZrO₂, Ga₂O₃, and Cr₂O₃. ^{22–24}

For the synthesis of conventional supported catalysts, the reactive metal is usually deposited on a carbon-based or an oxide support, such as Al₂O₃, SiO₂, TiO₂, CeO₂, ZnO, or ZrO₂ (Figure 1a), for enhanced dispersion.²⁵ The conventional catalytic supports influence the morphology, activity, and adsorption properties, as well as the dispersion, of the metal phase.²⁶

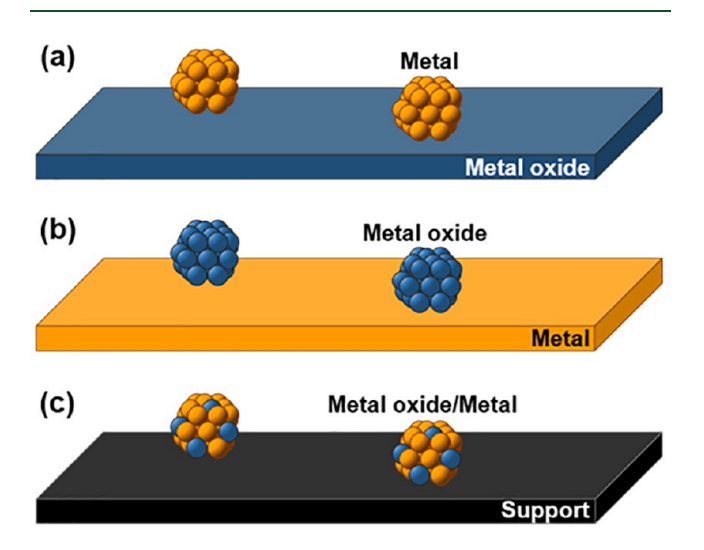


Figure 1. Illustration of (a) a traditional oxide-supported metal catalyst (M/MO_x) , (b) an inverse metal-supported oxide catalyst (MO_x/M) , and (c) a supported inverse oxide/metal catalyst (MO_x/M) support).

Moreover, catalyst supports are also utilized to tune the electronic properties to yield better catalytic performance. Thus, selecting an appropriate support is essential for catalyst development. For example, nanosized metal oxide supports can improve the interactions with the metal, providing a high density of defects and edge or corner surface sites. ^{25,27,28} These observations have motivated researchers to design catalysts where the metal oxide is deposited onto an unsupported (Figure 1b) or supported metal surface (Figure 1c), often referred to as inverse metal oxide/metal catalysts or simply inverse catalysts. To generate inverse catalysts, metal oxides have often been incorporated onto the surface of supported

metal nanoparticles via deposition techniques, such as atomic layer deposition (ALD). Other approaches involve the encapsulation of unsupported metal particles by metal oxides via core—shell methods. Another interesting strategy is based on the strong metal—support interaction (SMSI) effect, which involves the migration of the metal oxide support onto the surface of the metal nanoparticles, thereby creating inverted structures. Interestingly, when metal oxides are deposited on metal surfaces, they present different chemical and electronic properties than common bulk metal oxide supports. ^{27,29,30} These inverse catalytic materials have been reported to display improved redox properties, enhanced stability, increased number of interfacial sites, and oxophilic active centers. ^{31–33}

Earlier accounts highlighted the development of inverse catalytic systems. For example, Rodriguez and Hrbek discussed the use of inverse catalysts to elucidate the reaction mechanisms and the effect of metal oxides on the stability of the reaction intermediates.²⁵ The authors concluded that the practical application of these inverse catalysts would require the dispersion of oxide nanoparticles and metal on a support or the utilization of special synthesis procedures to prepare powder catalysts with an inverted configuration. Later on, Rodriguez et al. reviewed the practical applications of inverse catalysts, highlighting the strong oxide-metal interactions (SOMIs) that lead to significant perturbations in the electronic structure of both reducible and nonreducible oxides on inverse catalysts.³² Additionally, Zhang and Medlin described early design methods for synthesizing inverted nanoarchitectures.² While these earlier reviews focused on the general design of inverse catalysts to improve the catalyst stability and elucidate the reaction mechanisms, there is yet to be a thorough review focused on the use of inverse catalysts for CO₂ conversion. Moreover, recent efforts on CO₂ hydrogenation using inverse catalysts have displayed improved catalytic activity and stability, as well as enhancement in directing the product selectivity. Although there have been multiple literature reviews on CO₂ hydrogenation in recent years (Table 1), none of them exclusively addressed the use of inverse catalysts for CO₂ conversion. To this end, here we present the current state of the art of inverse catalysts for CO₂ hydrogenation with the desire to guide future investigations. Emphasis is placed on the type of metal oxide, and the protocols used to synthesize these inverted catalytic structures. Furthermore, we compare the performance of traditional and inverse catalysts for CO₂ hydrogenation, with a focus on the reaction mechanism and products formed. Lastly, future directions and areas for further study are proposed.

2. METHODS FOR THE SYNTHESIS OF INVERSE CATALYSTS

This section provides a brief overview of the techniques employed for the synthesis of inverse catalysts, as these directly affect the morphology, composition, and catalytic performance. The synthesis of well-defined metal oxide—metal interfaces requires rigorous and carefully controlled strategies, as the approach selected to deposit and disperse the metal oxide onto the metal surfaces can play an essential role in the synergistic and promotional effects of the interfacial sites under reaction conditions. Among the different methods reported in the literature for the synthesis of inverse catalysts, here we summarize those methods based on encapsulation strategies, other novel approaches such as controlled surface reactions

Table 1. Recent Review Articles on Thermocatalytic Hydrogenation of ${\rm CO}_2$

, e			
topic	catalyst(s)	year	ref
bimetallic catalysts for CO ₂ hydrogenation to methanol	multiple (e.g., Ni-, Cu-, or Pd-based)	2022	34
insights into CO ₂ hydrogenation to methanol synthesis	multiple (e.g., Cu, Au, Ag, or Pd)	2022	35
In_2O_3 -based composite catalyst for CO_2 hydrogenation	In ₂ O ₃ -based	2022	36
CO ₂ hydrogenation to methanol over Cu-based catalysts	Cu-based	2022	37
role of metal—support interactions in CO_2 conversion to methanol	Cu-based, noble metal- based, metal—organic- framework-based	2021	29
CO ₂ hydrogenation to methanol over Cu-based nanocatalysts	Cu-based	2021	24
${ m CO_2}$ hydrogenation to methanol over ${ m In_2O_3}\text{-based}$ catalyst, from mechanism to catalyst development	In_2O_3	2021	10
CO ₂ hydrogenation to methanol over homo- and heterogeneous catalysts	multiple (e.g., Ru, Fe, or Cu)	2021	38
CO ₂ hydrogenation to value-added hydrocarbons	multiple (e.g., Ni, Co, or Pd)	2021	39
CO ₂ hydrogenation to CO, methanol, and hydrocarbons	multiple (e.g., Cu, Rh, or In_2O_3)	2021	40
CO ₂ hydrogenation to value-added hydrocarbons	multiple (e.g., Cu, Ni, Ru, or Pd)	2020	41
CO ₂ hydrogenation to methanol via heterogeneous catalysis	multiple (e.g., Cu, Pd, or In_2O_3)	2020	42
CO ₂ conversion using dual function materials	Ni-, Ru-, and Rh-based	2020	17
CO ₂ conversion using CeO ₂ -based catalysts	CeO ₂ -based	2020	43
CO ₂ hydrogenation to methanol and methane over carbon-based catalysts	carbon-supported cata- lysts	2020	44
CO ₂ hydrogenation to liquid fuels with heterogeneous catalysts	multiple (e.g., Co, Pd, Cu, or Ni)	2020	45
CO ₂ hydrogenation to methanol over heterogeneous catalysts	multiple (e.g., Cu, Pd)	2020	46
CO ₂ hydrogenation to liquid methanol	multiple (e.g., Re, Ru, or Pd)	2020	47
CO_2 hydrogenation to methanol over non-Cu-based catalysts	various non-Cu cata- lysts (e.g., Zn, Pd, Pt, or Au)	2020	48
CO ₂ hydrogenation to liquid hydro- carbons via tandem catalysis design	various (e.g., Cu, Pd, or Ni)	2020	49
CO ₂ hydrogenation to methanol over ZrO ₂ -based catalysts	ZrO ₂ -based	2019	50
${ m CO_2}$ hydrogenation to carbon-based products: a computational chemistry perspective	Au-based catalysts	2019	51
CO ₂ hydrogenation to methanol over heterogeneous catalysts	various (e.g., Cu, Pd, or La)	2019	52

(CSRs) and microemulsions, and techniques for synthesizing inverse model catalysts.

2.1. Encapsulation Methods. Encapsulation involves embedding metal in a metal oxide.⁶² In addition to improved catalyst stability, encapsulation methods have also been reported to induce functionalities and modify the catalytic activity. Here, we briefly discuss three encapsulation techniques, namely, strong metal—support interaction (SMSI), atomic layer deposition (ALD), and core—shell methods.

SMSI was introduced by Tauster et al. in the late 1970s to describe the modification of the chemisorption properties of certain noble metals in contact with transition metal oxides. These interactions occur at high temperatures and are characterized by migration of the oxide supports to the surface of the metal nanoparticles, thus creating inverted struc-

tures.^{29,64} Lunkenbein et al. described the formation of a ZnO_x overlayer induced by SMSIs on the industrial Cu/ZnO/ Al₂O₃ catalyst for methanol synthesis.⁶⁰ They reported that a reductive treatment in H2 led to the formation of a metastable "graphitic-like" ZnO_x layer consistent with SMSI and the creation of inverse ZnO_x/Cu interfaces. That inverse structure was understood to stabilize the Cu phase and create new active sites for the hydrogenation of CO₂ to methanol. Diez-Ramirez et al. optimized the calcination and reduction treatments for Cu/ZnO catalysts.⁶⁵ They concluded that calcination at 350 °C followed by reduction at 200 °C provided the highest yield of methanol at low temperatures (<225 °C) with negligible formation of CO. Although the reduction at 150 °C led to the formation of smaller Cu nanoparticles, the temperature was not enough to fully reduce Cu, leading to the presence of both Cu²⁺ and Cu¹⁺, which facilitated the formation of methane. On the other hand, increasing the reduction temperature to 400 °C led to the formation of CuZn alloy particles providing the lowest CO₂ conversion. However, those CuZn alloys were more selective to methanol at higher reaction temperatures (>200 °C). While it has been postulated that the presence of defects could play a role in stabilizing the ZnO_x species over the Cu nanoparticles, 66 further fundamental studies using spectroscopic techniques and density functional theory (DFT) calculations could provide more insights into the reaction mechanism on these inverted catalytic structures.

Owing to the progress observed over the last four decades in the semiconductor industry, increasing miniaturization has required atomic-level control;⁶⁷ and, as a result, atomic layer deposition (ALD) has also been used for the synthesis of inverse catalysts. ALD comprises a series of self-limiting reactions, in which alternating pulses of the reacting precursors are separated by an inert purge stream.⁶⁸ In order to achieve high loadings with ALD, it is common to subject the substrate to multiple deposition cycles.^{68,69} Several ALD-based catalytic materials have been reported in the literature for diverse applications, including fuel cells, CO2 reforming of methane, and biomass conversion. 70-72 For example, Seo et al. deposited TiO2 on Ni nanoparticles by ALD for CO2 reforming of methane (CH₄ + CO₂ \rightleftharpoons 2CO + 2H₂; ΔH_r° = +247 kJ mol⁻¹) at elevated temperatures.⁷² They observed that the inverse TiO₂/Ni catalyst displayed higher activity and stability, with a CO₂ conversion of 68% compared to 31% obtained with the bare Ni catalyst. Scanning electron microscopy (SEM) images of the bare Ni and the 5-cycle ALD TiO2/Ni catalysts after reaction are depicted in Figure 2. While the SEM analysis of these materials before reaction showed no noticeable changes in morphology, the SEM images postreaction (Figure 2) revealed the presence of small TiO₂ nanoparticles on the Ni surface with a surface coverage of 7.2%. In addition, they claimed that the presence of TiO₂ islands suppressed the coke formation by disrupting the large Ni ensembles on the surface. Moreover, it was hypothesized that the TiO2-Ni interfacial sites contributed to the improved activity of the inverse catalyst.

Some advantages of the ALD method include uniformity and control of processing at low temperatures, stoichiometric control, and an inherent film quality associated with self-limiting reactions.⁷³ However, this technique also presents some challenges, such as low rate of deposition, use of expensive precursors and specialized equipment, high material waste rate, and difficulties in scale-up.⁷³ Nonetheless, ALD of oxides on metals has become a robust technique for the

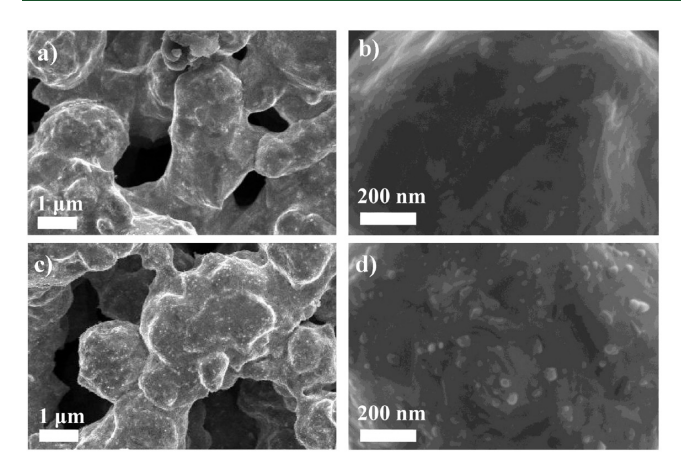


Figure 2. SEM images of the bare Ni catalyst at (a) low and (b) high magnification and ${\rm TiO_2/Ni}$ inverse catalyst at (c) low and (d) high magnification, showing the presence of ${\rm TiO_2}$ nanoparticles over the Ni surface. Peprinted with permission from ref 72. Copyright 2013 Elsevier.

synthesis of inverse catalysts. This is due to the advances in this technique, such as the ability to tune and control nanostructures, uniformity of the oxide layer, and atomic-level control of the synthesis protocol.

Likewise, core-shell techniques, in which an oxide shell covers a metal core, have been repeatedly employed to synthesize inverse catalysts. For example, Cargnello et al.⁷⁴ developed a method to synthesize Pd@CeO2 core-shell catalysts by reacting a cerium alkoxide with Pd particles stabilized by 11-mercaptoundecanoic acid, with subsequent partial protection of the alkoxy ligands and controlled hydrolysis to obtain dispersible Pd@oxide structures. Later, Bakhmutsky et al. used the same method to encapsulate Pd and Pt metallic cores with different oxide shells (CeO2, TiO2, and ZrO₂) (Figure 3). Those core-shell nanoparticles were then deposited on Al₂O₃, and their catalytic activity was studied in the water-gas shift (WGS) reaction (CO + $H_2O =$ $CO_2 + H_2$; $\Delta H_r^{\circ} = -41.2 \text{ kJ mol}^{-1}$). Interestingly, they observed that the reducibility of the oxide shell affected the stability of the catalyst, being ZrO2 the less reducible oxide, resulting in the most stable inverse catalyst.

Similarly, other inverse core—shell catalysts have also been reported in the literature. For example, Chen et al. 76 employed a colloidal method to synthesize Au@TiO $_2$ core—shell catalysts

that presented high thermal stability compared to similar materials prepared by impregnation. On the other hand, Forman et al.⁷⁷ and Park et al.⁷⁸ utilized microemulsion approaches to prepare silica-coated Pd cores. In both reports, those SiO2@Pd catalysts exhibited enhanced stability against sintering during the hydrogenation of acetylene. The Stöber synthesis technique is also a prevalent approach for synthesizing core-shell inverse catalysts. 79 This technique typically involves the ammonia-catalyzed hydrolysis and condensation of tetraethylorthosilicate (TEOS) in alcohol-water mixtures and has been particularly exploited for the development of structures in which a silica shell is grown around a metal core. 80-82 Recently, Gioria et al. designed a tandem catalyst using core-shell methodologies for the hydrogenation of CO₂ to methane and light hydrocarbons.⁸³Figure 4 shows some SEM and transmission electron microscopy (TEM) images to illustrate the complex synthesis protocol. First, they synthesized a silica core using the Stöber method (Figure 4a), followed by functionalization of the surface with amino groups (Figure 4b) and the formation of Pt nanoparticles on the surface by the strong electrostatic adsorption (SEA) method (Figure 4c,d). Next, a mesoporous silica shell was grown over the Pt-decorated silica core using a sol-gel method (Figure 4e,f), after which colloidal Co nanoparticles were incorporated onto the silica shell (Figure 4g,h). This strategy allowed for spatial control of the metallic sites and facilitated the occurrence of consecutive reactions on a single catalytic material. It was postulated that CO₂ reacted with H₂ on the Pt surface to produce mainly CO. Then, CO diffused to the Co sites, where it was hydrogenated to produce methane and light olefins, which are high-value-added products. However, although Pt agglomeration was not observed due to the protection from the silica shell, partial migration and coalescence of the Co nanoparticles were reported after prolonged time on stream. Nevertheless, this approach of tandem catalysis using inverted structures is a very interesting concept to facilitate the study of reaction systems at different space and time scales.

However, one of the main challenges of the use of coreshell structures can be the difficult access of the reactants to the active sites due to mass transfer limitations. To mitigate these challenges, material properties, such as the shell thickness, porosity, and presence of cavities within the shell, should be optimized. ⁸⁴ In addition, as current state-of-the-art core—shell synthesis protocols involve complex procedures and

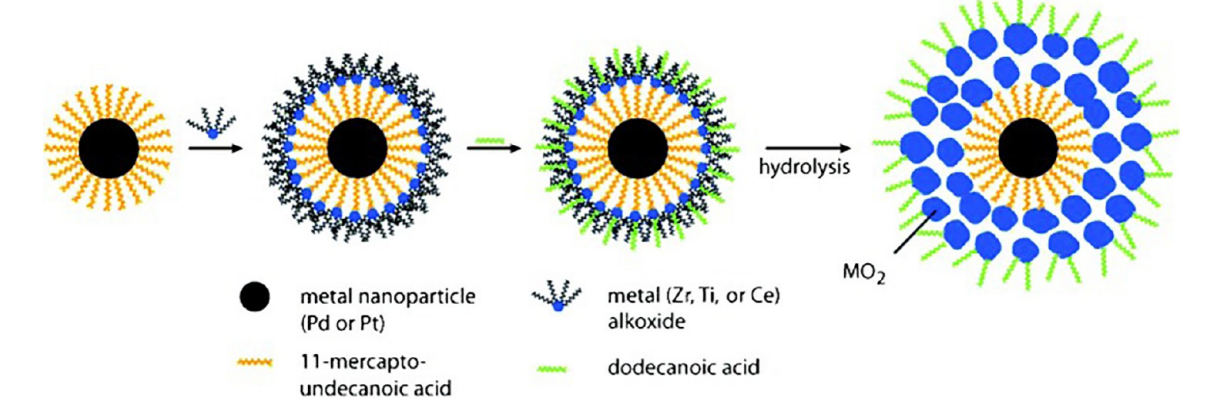


Figure 3. Stepwise representation of the procedure to prepare metal@oxide nanostructures.⁷⁵ Reprinted with permission from ref 75. Copyright 2012 John Wiley and Sons.

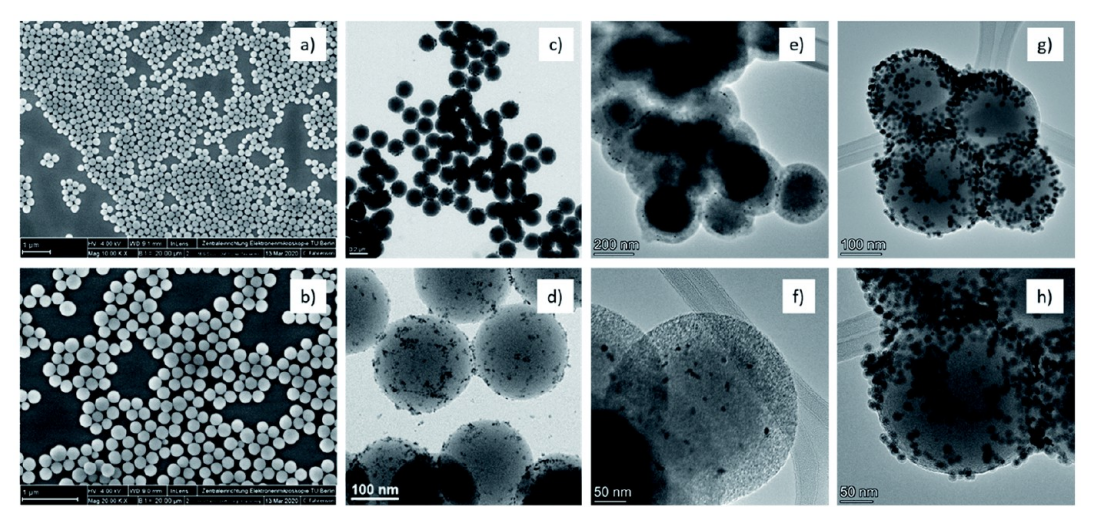


Figure 4. SEM and TEM images of (a) SiO₂ cores, (b) SiO₂-NH₂, (c, d) SiO₂-Pt, (e, f) SiO₂-Pt@m-SiO₂, and (g, h) SiO₂-Pt@m-SiO₂-Co. Reprinted with permission from ref 83. Copyright 2021 Royal Society of Chemistry.

multistep pathways, future research efforts should be directed toward developing cost-effective and scalable preparation methods

2.2. Controlled Surface Reactions (CSRs) and Microemulsions. More recently, controlled surface reactions (CSRs) have been used to synthesize oxide/metal inverse and bimetallic catalysts. 85-88 This technique typically involves the use of an organometallic precursor to deposit a metal oxide (or metal) onto metal nanoparticles via a facilitated surface reaction route. The main advantages of this method are that it can be performed in solution without requiring expensive high vacuum systems and that it leads to well-defined bimetallic or inverse catalysts with a narrow particle size distribution. 86 For example, Ro et al. reported the use of CSR to deposit zirconia (ZrO₂) on undercoordinated Cu sites for the hydrogenation of CO2 to methanol and the conversion of ethanol to ethyl acetate.⁸⁷ This technique allowed for the synthesis of welldefined Cu-ZrO2 interfacial sites, which improved the conversion and selectivity in both reactions. Also, Carrasquillo-Flores et al. deposited molybdenum oxide (MoO_x) on silica-supported gold nanoparticles (Au/SiO₂) using a modified CSR method for the RWGS reaction (eq 1).89 This led to the formation of Au–MoO_r interfacial sites, which were quantified by Fourier-transform infrared spectroscopy (FTIR) of CO uptake and shown to be an order of magnitude more active than Au sites for the RWGS reaction.

In contrast, the microemulsion technique is a synthesis method that consists of a thermodynamically stable dispersion of two immiscible solutions, one containing the metal precursor(s) and the other containing a precipitating agent. A similar approach may also involve the addition of a precipitating agent directly to an emulsion containing the metal precursor. 54,90 This method has proven notable advantages, such as the ability to produce sized-controlled small particles (5-50 nm) with a narrow particle size distribution, the possibility of recovering bimetallic nanoparticles at room temperature, and more importantly, high surface area support and well-dispersed active phase systems. 54,91,92 As a result, microemulsion techniques have also been used to synthesize inverse catalysts. Recently, Wang et al. 93 synthesized a series of ZnO/Cu inverse catalysts using a microemulsion method by varying the Zn/Cu molar ratio in

the precursor solution. Owing to the inverted structure, the surface exhibited a lower Cu/Zn molar ratio than that of the bulk phase. From X-ray diffraction (XRD) analysis, the particle sizes of both ZnO and Cu were evaluated using the Scherrer equation at $2\theta = 36.2^{\circ}$ and 43.3° , respectively. The Cu particle size obtained was as follows: ZnO/Cu (4:6) < ZnO/Cu (5:5) < ZnO/Cu (3:7) < ZnO/Cu (2:8) < ZnO/Cu (1:9), being ZnO/Cu (4:6) the catalyst with Cu nanoparticles of smaller size. However, no apparent differences were observed in the particle size of ZnO, thus indicating that this method was only effective for tuning the Cu particle size. Microscopic analysis revealed the presence of ~20 nm ZnO particles dispersed on a flake-like Cu surface, which was in agreement with XRD results. The series of ZnO/Cu catalysts was studied in the hydrogenation of CO₂, being ZnO/Cu (4:6) the most active catalyst with a methanol yield of 2.8 mmol $g^{-1}\ h^{-1}$ at 250 $^{\circ}C$ and 2 MPa. Remarkably, the unique nature of the inverse structure limited the presence of highly dispersed Cu sites, which are otherwise favorable for CO production rather than methanol.

However, the high cost of the reducing agents (e.g., tetramethylammonium hydroxide (TMAH), sodium borohydride (NaBH₄) and hydrazine (N₂H₄)), may limit the immediate industrial applications of these catalysts. In addition, the separation and recovery of the catalyst from the microemulsion is also a major challenge. ⁵⁴ Unfortunately, the presence of residual precipitant may also have an unpredictable effect on the activation of the catalyst, which makes this method less attractive than others for the synthesis of inverse catalysts.

2.3. Techniques to Synthesize Model Catalysts. Model catalysts, which are composed of single-crystal surfaces, have been extensively studied to understand the nature of the oxide—metal interfaces. Owing to the homogeneity of single-crystal surfaces, it is easier to examine the morphological effect and surface properties of the oxide—metal interfaces in these model catalysts than in technical metal/oxide catalysts that are more heterogeneous. These model catalysts are usually investigated under ultrahigh vacuum (UHV) conditions ($<10^{-9}$ Torr) to ensure a clean surface, and preparation schemes usually involve the physical vapor deposition of the metal. This reactive deposition is usually performed under an

oxygen atmosphere to create a metal oxide, followed by an annealing step to order the metal oxide particles. Alternatively, oxidation is sometimes conducted after depositing the metal to form alloyed structures. ⁹⁵ In the literature, there have been reported numerous inverse structures based on model catalyst design for the hydrogenation of ${\rm CO_2}^{27,94,95}$ As techniques to synthesize inverse catalysts at large scale develop, results from model and technical catalysts will enable the development of effective and industrially deployable materials.

Although most model catalysts attempt to mimic conventional industrial catalysts, there still exists a material gap between planar model catalysts and high surface area supported catalysts and a pressure gap between conventional reaction systems and the UHV conditions associated with model catalyst studies.⁹⁴ To overcome the material gap challenge, researchers have developed techniques to create well-characterized model catalysts on ultrathin metal oxide surfaces, thus enabling the investigation of support-metal interactions.⁹⁴ Regarding the pressure gap, systems have been developed whereby a reactor is connected to an UHV system, allowing for sample transfer between the two regimes for surface characterization before and after reaction without exposure to air. 94 However, further investigations are required with these model systems, as a challenging aspect of the surface science of inverse catalysts is the study of submonolayer structures, which are discontinuous yet very relevant to reactions that occur at the metal-oxide interfaces. To this end, several advanced techniques and instrumentation have been developed; notably, the use of scanning tunneling microscopy (STM) has recently helped to resolve some of these complexities. ²⁷Table 2 shows a summary of the different synthesis methods here discussed, with process description, commonly used oxides, and associated benefits and challenges of each method.

3. INVERSE CATALYSTS FOR CO₂ HYDROGENATION

Metal—metal oxide interfaces in traditional heterogeneous catalysts have been identified as active sites for ${\rm CO_2}$ hydrogenation. Although many catalyst supports are thought to be inert, it is well-known that they can contribute to the catalytic activity through the creation of active metal—oxide interfacial sites. ^{96,97} Hence, oxides that have been traditionally used as catalyst supports have also been deposited on metals to investigate the catalytic activity of inverse systems. The most commonly used metal oxides include cerium, zinc, indium, and zirconium oxides. In this section, we analyze some inverse systems that use these and other metal oxides for the hydrogenation of ${\rm CO_2}$.

3.1. Inverse CeO_x -Based Catalysts. Cerium oxide (CeO_x) -containing catalysts have been extensively studied in several chemical reactions. $^{31,53,95,98-101}$ A significant characteristic of ceria is the generation of oxygen vacancies due to the $Ce^{4+} \leftrightharpoons Ce^{3+}$ redox transformation that leads to a modification of the electronic properties. 99 Ceria-supported catalysts have proven to be effective for the hydrogenation of CO, resulting in the production of either light hydrocarbons (C_1-C_5) , alcohols, or other oxygenates, depending on the reaction conditions. $^{102-105}$ It is understood that the activation of CO by oxygen vacancies and the ability of the metal—oxide interfacial sites for chain growth are responsible for the high selectivity to methanol obtained with catalysts containing ceria. 106 Considering that CO has been postulated to be an intermediate during CO_2 hydrogenation, it is important to discuss the

Table 2. Summary of the Synthesis Methods, Process Description, And Commonly Used Oxides, with Associated Benefits and Challenges

synthesis cate- gory	methods	process description	common oxides	benefits	challenges
encapsulation	SMSI	migration of a reducible oxide over a metallic surface deposition of a thin oxide layer over a metallic surface via self-limiting reactions	TiO_2 , ZnO Al_2O_3 , TiO_2 , ZnO	modification of the catalytic activity and selectivity conformal thin layers, molecular control for tuning catalytic properties	selective to few oxide supports, requires high temperature treatments expensive precursors and vacuum, slow deposition rates, scale up difficulties
	core—shell	growing of an oxide shell around a metallic core	CeO ₂ , TiO ₂ , ZrO ₂ , SiO ₂	more versatile technique (allows the use of many different oxides)	more versatile technique (allows the use of many different complex synthesis protocols, can exhibit mass transfer limitations oxides)
others	CSR	utilization of organometallic precursors to deposit metal oxide via surface reactions	${ m ZrO}_2, \ { m MoO}_x$	performed in solution (does not require excessive vacuum), creates well-defined particles with narrow particle size distribution	requires the use of specific organometallic precursors, usually requires cyclic multistage deposition for increased loading
	microemulsions	involves the use of two microemulsions, one containing the metal precursors and other with the precipitating agent	ZnO	controlled morphology with narrow size distribution, low operating temperatures, less effect of the support on particle formation	high cost of precipitant, difficulty of separation and recovery of the catalyst from the medium, residual precipitant in the catalyst can negatively influence the activity
model catalysts	model catalysts physical vapor deposition	metal deposition in an O_2 atmosphere onto a clean ZnO, CeO _x crystal surface		homogeneous crystal surfaces, highly applicable to study surface science and reaction mechanisms	requires ultrahigh vacuum, material gap with conventional practical catalysts

advances in the use of cerium-based inverse catalysts for CO hydrogenation, as the conclusions eventually motivated the synthesis of similar catalysts for CO_2 hydrogenation. Recently, Salcedo and Irigoyen used first-principles microkinetic modeling to elucidate the prevalence of a combined redox-associative route for the WGS reaction on pure ceria. ¹⁰⁷ Their results not only corroborated the role of ceria as previously reported but also motivated further studies with similar catalysts for the WGS reaction under mild conditions.

Hu et al. recently tuned a Cu-Zn catalyst with cerium oxide $(CuZnCeO_x)$ to improve the CO_2 conversion to CO and methanol. The catalyst was synthesized via a parallel flow co-precipitation method in which the metallic precursor solutions and a precipitant (Na₂CO₃ solution) were added dropwise to a cetyltrimethylammonium bromide (CTAB) solution (dispersing agent) under stirring, after which the catalyst was recovered by filtration, dried, and calcined. Interestingly, the authors observed that the ceria-doped catalyst exhibited higher selectivity toward methanol, up to 83.1% at 200 °C. While the Cu sites were hypothesized to play a critical role in H₂ activation, CeO_x was responsible for strongly adsorbing CO2 due to increased basicity and the presence of oxygen vacancies. Furthermore, CeO_x enhanced the dissociative adsorption of H2, promoting the spillover of atomic hydrogen onto the Cu surface, resulting in a synergistic effect. These properties led to an enhanced performance and a higher selectivity to methanol. Ceria has also been used as a promoter to improve the activity of a Ga2O3 catalyst for the hydrogenation of CO₂. However, in this case, the catalyst demonstrated improved activity in the RWGS reaction (eq 1) to produce CO. The authors concluded that the presence of CeO₂ led to the generation of more bicarbonate species, an intermediate that thermodynamically favors the RWGS reaction. CO₂ temperature-programmed desorption (CO₂-TPD) experiments revealed that the formation of bicarbonate species was more favored on the CeO₂-promoted Ga₂O₃ catalyst than on pristine Ga₂O₃. Then, FTIR and Raman spectroscopy measurements confirmed that the presence of increased oxygen vacancies on the ceria-doped catalyst facilitated the CO2 activation to bicarbonate species via interaction with surface hydroxyl groups. Another example was provided by Damyanova and Bueno, 110 who studied the effect of ceria loading and size on a CeO₂-Al₂O₃-supported Pt catalyst and the ceria-metal interactions during the reforming of CO₂ to CH₄ (eq 2). Interestingly, they observed that ceria affected the reducibility of the Pt surface and prevented the deactivation by gasification of coke deposits. 110 The modification of the reducibility of Pt was attributed to the facile redox transformations discussed earlier, which in turn facilitated a higher dispersion of Pt on the catalyst support.

Model inverse ceria-containing catalysts have generally been synthesized using the techniques described in section 2. For instance, Kaemena et al. extensively studied the growth and morphology of an inverse catalyst synthesized by the deposition of ceria on Ru(0001) facets. Different monolayers (MLs) of ceria (each having a thickness of 3.12 Å) were grown in situ under UHV conditions by reactive molecular beam epitaxy at substrate temperatures between 360 and 1000 °C using an electron beam evaporator under preset oxygen background pressures between 1×10^{-8} and 5×10^{-7} Torr. Their results showed the possibility of controlling the size of the ceria islands, nucleation density, and oxidation state by adjusting the conditions, such as the oxygen partial pressure

between 2×10^{-7} and 5×10^{-7} Torr. Furthermore, the characterization of the resulting catalyst by low-energy electron diffraction (LEED) demonstrated that the oxide-metal interface was well ordered, as shown in Figure 5. The well-

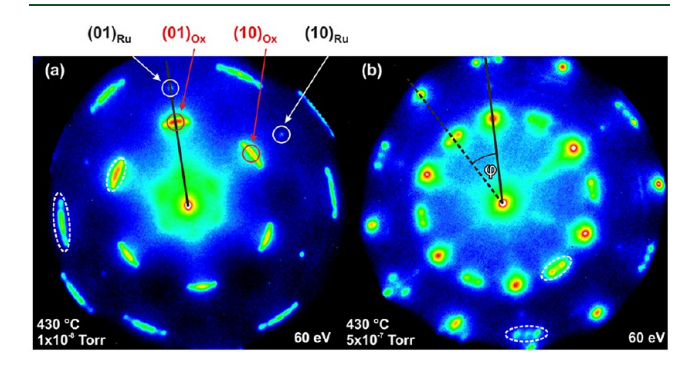


Figure 5. LEED images of 3 MLs of ceria grown at 430 $^{\circ}$ C and an oxygen partial pressure of (a) 1×10^{-8} Torr and (b) 5×10^{-7} Torr. Reprinted with permission from ref 111. Copyright 2013 American Chemical Society.

ordered sites and single crystal surfaces provided by model catalysts enable the elucidation of the activity on specific metal sites and interfaces without defects, multiple active sites, surface heterogeneity, and other complexities present in high surface area supported catalysts. For this reason, model inverse catalysts have proven to be ideal for surface science studies.

Surface science studies have thus been employed to better understand the morphology and defects on ceria films. As an example, Lu et al. also used STM analysis in combination with LEED and Auger electron spectroscopy (AES) to study the growth of ceria overlayers on Ru(111). 112 CeO₂ films were added by physical vapor deposition under 1×10^{-7} mbar of oxygen and postoxidation at 980 K to ensure that it covered the entire metal surface. In addition to reactivity studies over ceria and metal/ceria, the film morphology and surface defects we also studied by STM. For example, Figure 6 clearly shows

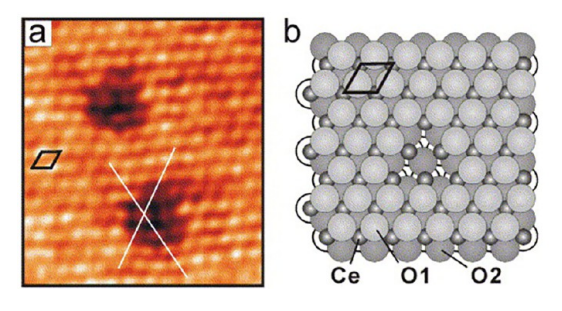


Figure 6. (a) STM image and (b) corresponding schematic representation of the defects observed on the ceria films. Reprinted with permission from ref 112. Copyright 2006 Elsevier.

defects attributed to three missing oxygen atoms in the top layer due to the formation of oxygen vacancies on the ceria surface. In addition, they observed the presence of undercoordinated terrace and step sites by STM. These undercoordinated sites usually contribute significantly to the activity and can also be subjected to deactivation modes like leaching and sintering due to presence of fewer neighboring atoms.

Inverse ceria-metal catalysts synthesized by the aforementioned methods (deposition of metallic Ce in a low-pressure oxygen environment) have been employed for the hydro-

genation of CO_2 . Metal—oxide interfaces on CeO_x/Cu were demonstrated to provide improved chemical properties, as evidenced by Graciani et al. They prepared $CeO_2/Cu_2O/Cu(111)$ by vapor deposition of cerium onto Cu(111) in an oxygen atmosphere, forming thick layers and rough surfaces of ceria islands on Cu_2O step edges, as depicted by STM studies (Figure 7). The hydrogenation of CO_2 using $CeO_x/Cu(111)$

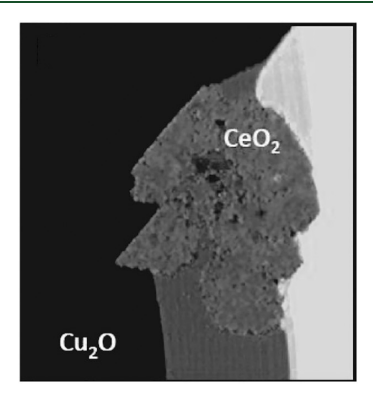


Figure 7. STM image of a synthesized CeO_x/Cu(111) surface.¹⁰¹ Reprinted with permission from ref 101. Copyright 2014 American Association for the Advancement of Science.

with ceria covering about 20% of the Cu surface resulted in a turnover frequency (TOF) of 1.3 molecules of methanol per active site per second at 300 °C. In the investigation of the reaction mechanism, they observed that the inverse $\text{CeO}_x/\text{Cu}(111)$ catalyst induced a reaction pathway via the formation of carboxylate ($\text{CO}_2^{\delta-}$) species. Using ambient-pressure X-ray photoelectron spectroscopy (AP-XPS), they observed that those $\text{CO}_2^{\delta-}$ species were unstable under exposure to H_2 at 200 °C. Interestingly, the presence of $\text{CO}_2^{\delta-}$ species provided a 200-fold increase in the TOF of methanol when compared to the monometallic Cu(111) catalyst.

Using similar CeO_x/Cu(111) and ZnO/Cu(111) catalysts, Senanayake et al. 113 investigated the particular role of the metal-oxide interface and the Ce3+ sites during CO2 hydrogenation. To do so, they varied the CeO_r and ZnO coverage of the Cu metal surface to ascertain that the active centers responsible for the reaction were indeed the metaloxide interfacial sites. Figure 8 shows that the maximum methanol production occurred when 20% of the Cu surface was covered with ZnO or 30-50% with ceria before decreasing at higher coverages. Those catalysts were prepared by depositing metallic Zn and Ce onto a clean Cu(111) surface under 5×10^{-7} mmHg of O₂ at 326 °C to form ZnO/CuO_x/ Cu(111) and $CeO_2/CuO_r/Cu(111)$, respectively. Then, further reduction under H2 or exposure to a CO2/H2 reactant mixture transformed these surfaces into ZnO/Cu(111) and $CeO_x/Cu(111)$, creating inverted structures.

As seen in Figure 8, the catalytic activity completely disappeared at full coverage, clearly indicating that the reaction took place at the metal (Cu)—oxide (CeO_x or ZnO) interface and not on the oxide surface. Likewise, AP-XPS studies showed that the maximum number of $\mathrm{CO_2}^{\delta-}$ species was obtained when the Cu surface was 20–30% covered by oxide, while it was not detected at full metal coverage.

3.2. Inverse ZnO-Based Catalysts. The interactions between the components of the Cu/ZnO/Al₂O₃ commercial catalyst for CO₂ hydrogenation to methanol were investigated by Lunkenbein et al., ⁶⁰ who highlighted the role of ZnO as a

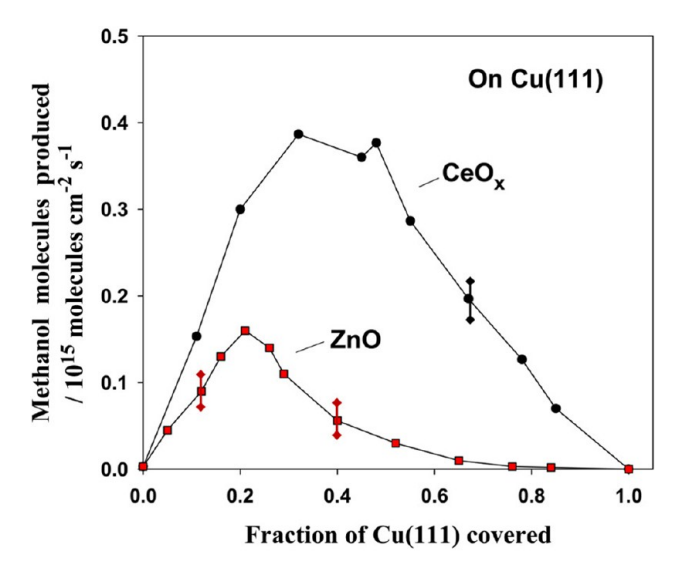


Figure 8. Rate of methanol formation from CO₂ as a function of the fraction of Cu covered by ceria or zinc oxide. ¹¹³ Reprinted with permission from ref 113. Copyright 2016 American Chemical Society.

Cu-stabilizing agent. Scanning transmission electron microscopy (STEM) analysis depicted the formation of a ZnO overlayer on the Cu nanoparticles due to SMSI. In recent reports, ZnO overlayers proved to create highly active interfacial sites with the metal nanoparticles and the support. The observations on the promotional effect of ZnO on Cu-based catalyst for methanol synthesis has motivated other studies on inverse ZnO/Cu catalysts to maximize the synergistic effects. 116 As discussed in the introduction, metal-oxide interactions are more significant when the oxide is deposited onto the metal rather than in metal-on-oxide arrangements. Reichenbach et al. 117 used gradient-corrected DFT to study the hydrogenation of CO₂ over inverse ZnO/Cu catalysts and demonstrated that the reaction proceeded through the formate pathway, unlike when other metal oxides, such as ceria and zirconia, are deposited on copper. Therefore, it can be concluded that the reaction mechanism for methanol formation over these inverted catalysts can be modified by the choice of metal oxide employed. The production of methanol from CO2 without a measured/detected CO intermediate has also been reported in numerous studies with the industrial Cu/ZnO/Al₂O₃ catalyst. ^{114,117,118}

In a similar study, Palomino et al. 119 synthesized ZnO/ Cu(100) and ZnO/Cu(111) catalysts for CO₂ hydrogenation to methanol. These catalysts were synthesized by deposition of metallic zinc in an oxygen environment onto a clean Cu substrate at 330 °C to form ZnO/CuO_x/Cu(111) and ZnO/ CuO_x/Cu(100). Then, these were transformed into ZnO/ Cu(111) and ZnO/Cu(100) after exposure to H₂ at 80-130 °C. To measure the catalytic activity, the reactants (0.5 atm CO₂ and 4.5 atm H₂) were fed into the reactor at room temperature, and the mixture was heated to the reaction temperature (230-330 °C). Several ZnO coverages were tested, and the highest activity was found at approximately 20% coverage in both cases, as illustrated in Figure 9. It was hypothesized that a small mono- or bilayer of zinc oxide was present on top of the metal and that the activity of those layers was enhanced by their size and interaction with Cu at the ZnO-Cu interface. AP-XPS studies conducted on Cu under

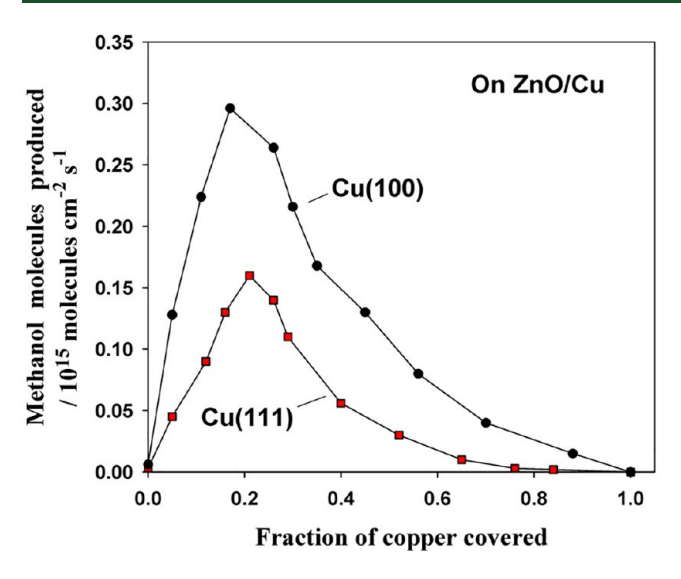


Figure 9. Methanol production rate on Cu(100) and Cu(111): Effects of the ZnO coverage (4.5 atm H_2 , 0.5 atm CO_2 , 550 K). Reprinted with permission from ref 119. Copyright 2018 American Chemical Society.

flow of H_2 and CO_2 revealed the presence of $CO_2^{\delta-}$ species, which disappeared from the Cu surface upon heating to 500 K. However, the AP-XPS spectra recorded with ZnO/Cu surfaces exposed to the same reactants revealed not only the presence of $CO_2^{\delta-}$ but also formate species, thus highlighting the significant role of the ZnO–Cu interface that accelerates the CO_2 binding and transformation. To properly understand the synthesis of methanol from CO_2 with the inverse ZnO/Cu₂O/Cu(111) catalyst, Orozco et al. exposed the catalyst along with Cu_2O/Cu to methanol and conducted spectroscopic studies using AP-XPS. The 3D view of the ZnO islands on the $CuO_x/Cu(111)$ surface is depicted in Figure 10. They

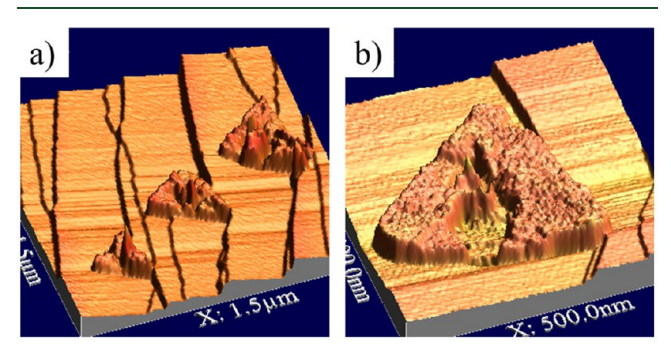


Figure 10. 3D view of the inverse $ZnO/CuO_x/Cu$ catalyst depicting the presence of ZnO islands on the $CuO_x/Cu(111)$ substrate: (a) 1500 nm scale and (b) 500 nm scale. Reprinted with permission from ref 28. Copyright 2021 American Chemical Society.

observed two prominent species that correspond to the methoxy ($\mathrm{CH_3O}$) and formate (HCOO) groups formed from the reaction of adsorbed $\mathrm{CH_3O}$ and O atoms from the CuO_x substrate with some residual CH_x . Interestingly, it was observed that the presence of ZnO led to the stabilization of $\mathrm{CH_3O}$, inhibiting its conversion to HCOO. This was suggested to be the result of the increased bond strength of O atoms to surface Zn compared to those on the Cu surface. Then, further analysis using STM and DFT pointed the ZnO regions as the preferential sites for adsorption of $\mathrm{CH_3O}$. However, most of

the CH₃O groups were observed to disappear upon heating to 450 K, which is the temperature at which methanol starts forming from CO₂ hydrogenation.

Recently, Wang et al. ⁹³ synthesized a series of ZnO/Cu catalysts with different Zn/Cu ratios by the microemulsion method. Catalyst characterization using XRD, TEM, and $\rm H_2$ temperature-programmed desorption ($\rm H_2\text{-}TPD$) showed that Cu species were less dispersed than in a conventional Cu/ZnO catalyst. This observation is believed to be responsible for the higher CH₃OH selectivity (59 mol %) and lower CO selectivity in the hydrogenation of CO₂. As previously stated, the inverse catalyst with the ZnO/Cu ratio of 4:6 showed the highest CH₃OH yield (2.8 mmol g⁻¹ h⁻¹) at 2 MPa and 250 °C for 50 h. In contrast, a conventional Cu/ZnO catalyst with the same ratio exhibited a much lower CH₃OH selectivity with a methanol yield of 1.8 mmol g⁻¹ h⁻¹ at 3 MPa and 250 °C.

Two possible pathways have been postulated for the hydrogenation of CO_2 on ZnO-Cu-based systems. In some cases, it seems likely that the CO_2 hydrogenation mechanism over bifunctional catalysts involves the RWGS reaction followed by CO hydrogenation, while in other cases, it is believed that the reaction may proceed directly from CO_2 to methanol via a formate intermediate. These two possible reaction pathways are illustrated in Figure 11.

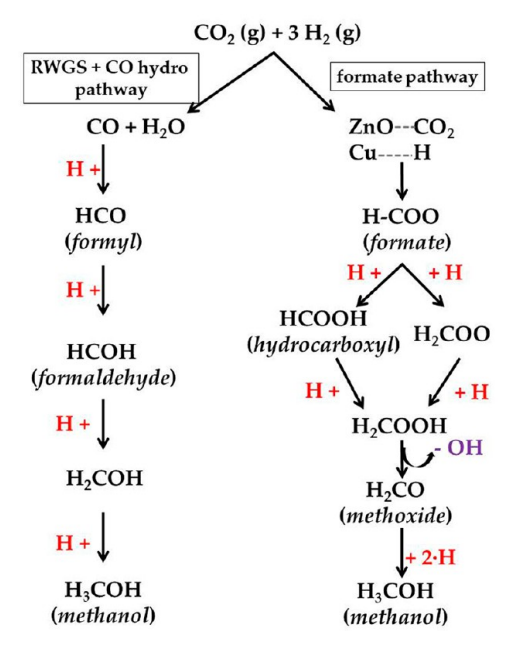


Figure 11. CO_2 to methanol mechanisms: RWGS + CO hydrogenation vs formate pathway. ¹²⁰

In a typical formate mechanism pathway, ¹²¹ CO₂ is adsorbed on the oxygen vacancies of metal oxide (e.g., ZnO) and H₂ undergoes dissociative adsorption on the metal surface (e.g., Cu); then adsorbed H interacts with carbon to produce a formate (HCOO) intermediate. After that, subsequent hydrogenation steps with the loss of a hydroxyl group generate methanol. On the other hand, in the RWGS + CO hydrogenation pathway, CO₂ is converted into CO, after which this is hydrogenated to methanol via formyl (HCO) and formaldehyde (HCHO) intermediates. The detailed mechanisms depend on the types of catalysts used and are well documented in greater detail elsewhere. ^{122–125} CO₂ hydrogenation to methanol on inverse catalysts may follow the above

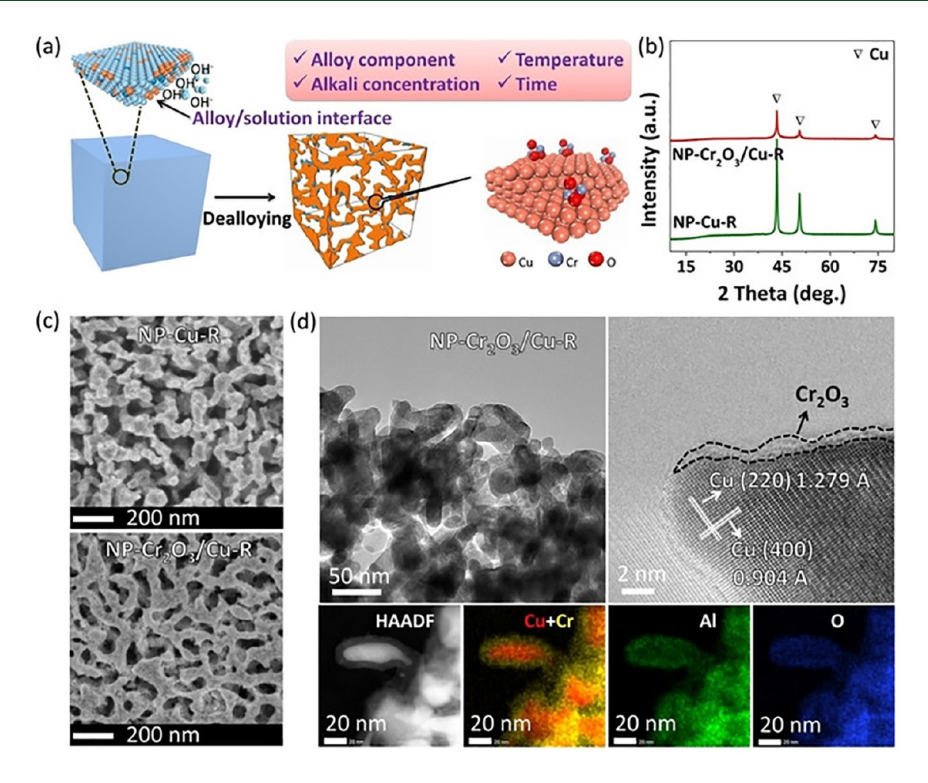


Figure 12. (a) Schematic of the dealloying process of CuCrAl alloy in an alkaline solution and the formation mechanism of the nanoporous Cr_2O_3/Cu catalyst and (b) XRD patterns, (c) SEM images, and (d) TEM images of the Cu and Cr_2O_3/Cu catalysts. Exprinted with permission from ref 61. Copyright 2019 John Wiley and Sons.

mechanisms or proceed via more complex routes depending on the chemical nature of the catalysts.⁹⁵

3.3. Other Inverse Catalysts Containing Cr₂O₃, ZrO_x, or CsO_x. Due to the multistep approaches and high temperature treatments for the synthesis of inverse catalysts discussed in previous sections, Shen et al.⁶¹ explored the use of a facile dealloying procedure to prepare inverse nanoporous (NP) Cr₂O₃/Cu catalysts for the RWGS reaction. To do so, they started with a ternary CrCuAl alloy and adjusted the alkali concentration, temperature, and time during the dealloying process (Figure 12a). XRD profiles and SEM images of the Cu and Cr₂O₃/Cu catalysts are presented in Figure 12b,c, respectively. The visible peaks were ascribed to Cu, while the absence of Cr₂O₃ peaks was attributed to the low crystallinity and content. TEM images (Figure 12d) showed the presence of a Cr₂O₃ overlayer on the Cu ligaments, which would likely allow for efficient electron transfer and provide a stable interfacial structure. The catalytic performance of the nanoporous Cr₂O₃/Cu catalyst was found to be twice that of the commercial Cu/ZnO/Al₂O₃ catalyst at low temperatures due to the unique structural properties (step and kink sites) of the oxide/metal interface and the nanopores, which enhanced the CO₂ activation and H₂ dissociation. However, unfortunately, this catalyst displayed poor stability due to surface restructur-

In other studies, zirconia has also proven to promote the performance of copper-based catalysts in the hydrogenation of ${\rm CO_2}$. The main reason for this improvement is the capacity of inhibiting byproducts (CO and CH₄) owing to the fine-tuning capability of reduced ${\rm Zr^{3+}}$ at the interface, which can bind the key reaction intermediates. ^{124,126} Based on these benefits, Wu et al. ¹²⁷ synthesized a series of inverse ${\rm ZrO_2/Cu}$ catalysts with different oxide/metal ratios via co-precipitation for ${\rm CO_2}$

hydrogenation to methanol. XRD analyses revealed that the ZrO₂ phase was amorphous with a particle size of around 1.2 nm. The reactivity tests showed that a catalyst with ZrO₂/Cu ratio of 0.1 (ZrO₂/Cu-0.1) provided the highest space time yield (STY) of CH₃OH at a rate of 524 g_{MeOH} $kg_{cat}^{-\bar{1}}$ h^{-1} (493 K, 3 MPa, and a H_2/CO_2 ratio of 3). Then, AP-XPS and operando diffuse reflectance infrared Fourier-transform spectroscopy (DRIFTS) studies revealed that ZrO2 existed primarily in a highly reduced state with formate and methoxy intermediates. These reaction intermediates were also observed to form and consume much faster on the inverse ZrO₂/Cu configuration than on conventional Cu/ZrO2, leading to a methanol STY 3.3 times higher than that with Cu/ZrO₂ (159 g_{MeOH} kg_{cat}⁻¹ h⁻¹). Although the CO₂ conversion was low (under 5%), the optimum ZrO₂/Cu-0.1 material with 10% ZrO₂ loading presented similar performance as the Topsoe catalyst, which is known for being one of the best commercial catalysts for methanol synthesis. 128 Zou et al. went a step further by promoting an inverse ZrO2/Cu catalyst with ZnO for the hydrogenation of CO₂ to methanol. Compared to the ZrO₂/Cu catalyst, the incorporation of 6 wt % ZnO increased the catalytic activity. Under the reaction conditions used (473 K, 2 MPa, and a H_2/CO_2 ratio of 4), the methanol STY was of 0.45 g_{MeOH} g_{cat}^{-1} h^{-1} , which is 2.3 and 1.3 times higher than those obtained with the ZnO-free analog and the conventional Cu-ZnO-ZrO₂ catalyst, as shown in Figure 13. The methanol STY obtained in this work is close to that reported by Wu et al.; 127 however, they performed the reaction at lower temperature and pressure, which represents an advantage for potential industrial application. ZnO was postulated to play a structural role, acting as a spacer that facilitates the reduction of the Cu particles promoting the hydrogen activation. In addition, the high Cu surface area

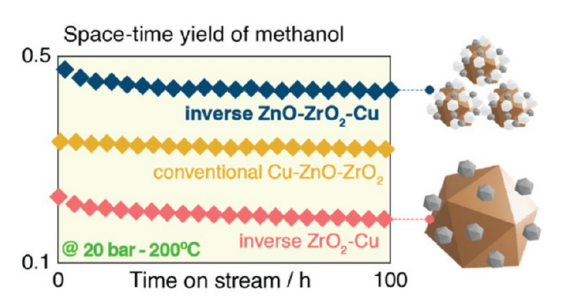


Figure 13. Comparison of STY of methanol $(g_{MeOH} \ g_{cat}^{-1} \ h^{-1})$ obtained with inverse $ZnO-ZrO_2-Cu$, conventional $Cu-ZnO-ZrO_2$, and inverse ZrO_2-Cu catalysts (473 K, 2 MPa, and H_2/CO_2 ratio of 4). ¹²⁹ Reprinted with permission from ref 129. Copyright 2022 American Chemical Society.

(small particles) contributes to enhanced interactions between ZnO, Cu, and ZrO₂ phases, leading to an improved catalytic activity.

To further elucidate the mechanism on the inverse ZrO₂based catalysts, Ma et al. reported the use of a model zirconia/ copper inverse catalyst (ZrO₂/Cu₂O/Cu(111)) for CO₂ hydrogenation. 130 The authors observed that the presence of ZrO₂ improved the CO₂ adsorption in the form of carbonate (COOO) species and facilitated the subsequent hydrogenation step through a formate (HCOO) intermediate that ultimately led to methoxy (CH₃O), which is the final precursor to methanol. This was attributed to the increased number of Cu-ZrO₂ interfacial sites that would facilitate the H spillover from the Cu sites to the intermediates bound on zirconia. Conversely, when no ZrO₂ was present on the catalyst, the RWGS reaction was dominant leading to the formation of CO. This study also highlighted the importance of oxide nanoparticles (ZrO₂) in modifying the reaction intermediates and directing the product selectivity.

Promoters (mostly alkali metals) have been shown to improve the activity of traditional catalysts for CO_2 hydrogenation. Recently, Hamlyn et al.¹³¹ synthesized copper-based catalysts with CsO_x nanostructures (1–3 nm range) as promoters for the hydrogenation of CO_2 to methanol. These catalysts were prepared by depositing cesium metal on $Cu_2O/Cu(111)$ and plain Cu(111) substrates at 650 K.

As in previous studies, STM and AP-XPS were used to study the morphology and chemical properties of the catalysts, presenting reconstruction of Cu_2O as shown in Figure 14. They found that $\text{CsO}_x/\text{Cu}_2\text{O}/\text{Cu}(111)$ was more reactive

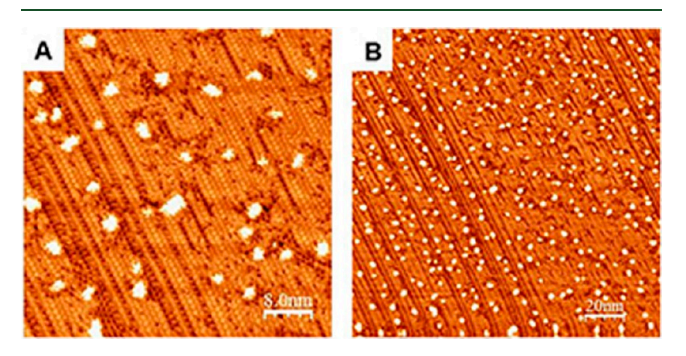


Figure 14. STM image of (A) $Cu_2O/Cu(111)$ surface before the deposition of CsO_x and (B) CsO_x deposited on the $Cu_2O/Cu(111)$ surface at 300 K.¹³¹ Reprinted with permission from ref 131. Copyright 2020 AIP Publishing.

toward CO_2 than $Cu_2O/Cu(111)$ or clean Cu(111), although none of those systems showed stability in the presence of H_2 , leading to the complete reduction of Cu_2O . They also observed that the $CsO_x/Cu(111)$ catalyst displayed the highest activity for CO_2 binding and dissociation, which suggests that CsO_x may not act as a simple promoter; if not that the CsO_x-Cu interface may be key in the formation of methanol or higher alcohols from CO_2 . Table 3 shows a summary of the inverse catalysts used for CO_2 hydrogenation and their synthesis methods, operating conditions, and reaction products and intermediates.

Overall, inverse catalysts have proven to be active materials for CO_2 hydrogenation. The presence of highly dispersed oxide nanoparticles on metallic substrates provides desirable interfacial interactions that have been shown to be beneficial in the formation of key reaction intermediates (e.g., formate) for methanol synthesis. Mechanistically, the proximity of neighboring sites allows for synergistic effects and spillover of reactive hydrogen species from metallic sites to interfacial sites where CO_2 is been activated. Model inverse catalysts in conjunction with advanced microscopy and spectroscopic methods, such as STM and AP-XPS, have given insights into these reaction systems and have potential to contribute to further rational catalyst design.

4. HYBRID OXIDE CATALYSTS

The catalytic activity can also be improved by dispersing metal oxides on oxide supports, and these catalysts are referred to as hybrid oxide catalysts. Tuning the size, shape, and chemical state of these catalysts can exert a significant influence on both the reactivity and the oxide—oxide interfacial activity by offering stable catalyst systems. Hecently, novel hybrid catalysts (e.g., $MnO_x/m-Co_3O_4$, 135 In_2O_3/ZrO_2 , 136,137 and $ZnO-ZrO_2$ hydrogenation to methanol.

Li et al. 135 reported that MnO_x/mesoporous-Co₃O₄ catalysts resulted in a high methanol yield at 523 K and 4 bar. Based on electron energy loss spectroscopy (EELS) and surface-sensitive X-ray absorption spectroscopy (XAS) analyses, they concluded that the active phase was the interface between the cobalt oxide surface layers and the MnO_x nanoparticles. Noteworthily, the TOF obtained with the hybrid MnO_x/m-Co₃O₄ catalyst was much higher (~0.85 s⁻¹) than that obtained with m-Co₃O₄ $(\sim 0.28 \text{ s}^{-1})$ or MnO_x/m-SiO₂ $(\sim 0.023 \text{ s}^{-1})$, which stresses the importance of the interfacial perimeter created on these hybrid structures. Furthermore, the methanol selectivity was significantly higher with the hybrid catalyst, with the additional unique feature of producing 10% ethylene via C-C coupling. They suggested that the good catalytic performance could be attributed to the reduction of CO₂ to CO species on the MnO₂ nanoparticles and further reaction of CO on the cobalt oxide surface to produce methanol and ethylene via chain growth. Surprisingly, when the catalyst was inverted (i.e., CoO_x nanoparticles deposited on a mesoporous MnO2 support), the catalyst was predominantly selective for CO, again highlighting the role that the nature and architecture of the interface plays in the catalytic activity.

Recently, In_2O_3 has also proven to be highly active for methanol synthesis from CO_2 . $^{137,139-141}$ It was evidenced from DFT calculations over a defective $In_2O_3(110)$ surface that the hydrogenation of CO_2 to HCOO was thermodynamically and kinetically favored. Then, similar to inverse oxide/metal catalysts, H_2CO is formed from the hydrogenation of

Table 3. Summary of Recent Inverse Catalysts for CO₂ Hydrogenation

catalyst	synthesis method	$\frac{\mathrm{H_2}}{\mathrm{CO_2}}$	reaction temperature (K)	main product	intermediate(s)
ZnO/Cu ¹¹⁷	computational study	а		methanol	formate
$ZnO/Cu(111)^{113}$	physical vapor deposition	9	500-600	methanol	formate
$ZnO/Cu(100)^{119}$	physical vapor deposition	9	500-600	methanol	formate
ZnO/Cu ⁹³	microemulsion method	3	523	methanol	not postulated
ZrO_2/Cu^{127}	co-precipitation method	3	453-493	methanol	formate and methoxy
Cr_2O_3/Cu^{61}	chemical dealloying of CrCuAl	4	673	CO (RWGS)	hydroxyl species
ZnO/Cu ¹³²	direct calcination of Cu@ZIF-8 at 623 K for 6 h	3	483-543	methanol	
$CeO_x/Cu (111)^{113}$	physical vapor deposition	9	500-600	methanol	formate and carboxylates
$\frac{\text{Cu/CeO}_x}{\text{TiO}_2(110)^{101}}$	co-deposition of Cu and ceria nanoparticles on ${\rm TiO_2}(110)$	9	500-600	methanol	formate
$Au/CeO_x/TiO_2^{133}$	CeO _x deposition in O ₂ atmosphere	7	573	methanol	via CO (RWGS)
$\frac{\text{CsO}_x/\text{Cu}_2\text{O}}{\text{Cu}(111)^{131}}$	deposition of Cs metal on $\mathrm{Cu_2O/Cu(111)}$ substrates at 650 K		450-600	methanol	
^a Not applicable.					

HCOO, followed by its hydrogenation to CH₃O. They concluded that the production of methanol replenishes the oxygen vacancies on the $In_2O_3(110)$ surface, while H₂ facilitates the generation of vacancies; thus, the reaction follows a mechanism involving the cyclic generation and consumption of oxygen vacancies, as shown in Figure 15.¹⁴²

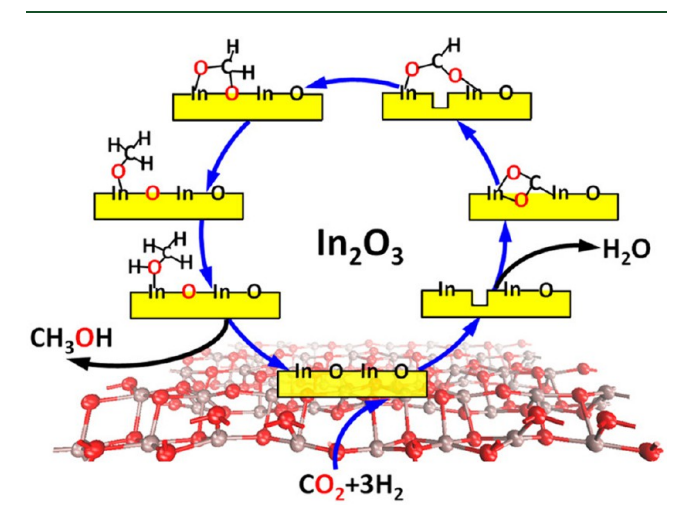


Figure 15. Cyclic consumption and generation of oxygen vacancies during methanol production over a defective ${\rm In_2O_3(110)}$ surface. ¹⁴²Reprinted with permission from ref 142. Copyright 2013 American Chemical Society.

Computational results revealed that the oxygen vacancies on the $\rm In_2O_3(110)$ surface were critical in the activation and hydrogenation of $\rm CO_2$ and facilitated the stabilization of key intermediates for methanol production.

 ${\rm In_2O_3/ZrO_2}$ catalysts synthesized by calcination of ${\rm In(OH)_3}$ were also found to be highly active, selective (100% methanol), and stable (1000 h) under industry-like conditions (573 K, 5 MPa, and a ${\rm H_2/CO_2}$ ratio of 4). Like in the case of traditional and inverse oxide/metal catalysts, the chemical and electronic state of the hybrid oxide catalysts can also be modified by addition of an alkali promoter. Additionally, Jiang et al. Additionally, Interestingly, they reported that the addition of 0.1% water increased the methanol selectivity by 20%. This was due to ${\rm H_2O}$ -induced oxygen vacancies, which

significantly improved the CO₂ adsorption capacity and the formation of InOOH intermediates, as detected by XPS, which correlated with the methanol production. Several other promoters have also been employed to boost the activity of In₂O₃, such as palladium, ¹⁴³ lanthanum, and yttrium. ¹³⁹ Also, there have been experimental investigations on the activity of In₂O₃ for the hydrogenation of CO₂ to methanol at elevated pressures. ¹⁴¹ For example, Sun et al. ¹⁴¹ developed a highly active and stable In2O3 catalyst for CO2 hydrogenation, thus corroborating the results obtained from theoretical studies. These catalysts were prepared by calcination of commercial indium(III) oxide powder at 500 °C for 5 h in air, and the reactions were performed at temperatures between 250 and 350 °C and pressures of 1-4 MPa. The results showed that CO₂ conversion increased with temperature and pressure (e.g., 0.1% at $250~^{\circ}\text{C}$ and 1~MPa and 9% at $350~^{\circ}\text{C}$ and 4~MPa), and the same trend was observed for the yield and rate of methanol production. However, the optimum results were obtained at 330 °C and 4 MPa, with CO₂ conversion of 7.13%, methanol yield of 2.82%, and a methanol formation rate of 3.69 mol_{MeOH} $h^{-1} k g_{cat}^{-1}$.

A ZnO-ZrO2 solid solution catalyst has also been investigated for the hydrogenation of CO2 to methanol. Wang et al. synthesized a series of highly selective and stable $ZnO-ZrO_2$ catalysts with different Zn/(Zn + Zr) molar ratios by co-precipitation. 138 These displayed excellent methanol selectivity above 85% and CO₂ conversion exceeding 10%. Also, the catalytic activity was observed to depend on the Zn/ (Zn + Zr) ratio, with an optimum performance at a Zn/(Zn +Zr) molar ratio of approximately 13%. Just like with other hybrid catalysts discussed above, the activity of the ZnO–ZrO₂ catalyst was superior to that of the individual oxides. Then, the authors demonstrated that the synergy between ZnO and ZrO₂, whereby H₂ is dissociatively adsorbed on the ZnO sites and CO2 is simultaneously activated on the neighboring ZrO2 sites, is responsible for the superior catalytic performance of these hybrid catalysts. In addition, these materials proved to be highly stable against sulfur-containing feeds, making the catalysts more suitable for industrial applications.

Additional metal oxides can also be incorporated as promoters to tune the reaction pathways. As an example, Wang et al. investigated the addition of WO₃ to a CuO–ZnO–ZrO₂ catalyst prepared by co-precipitation. ¹²⁸ Interestingly, they observed that both the CO₂ conversion and methanol

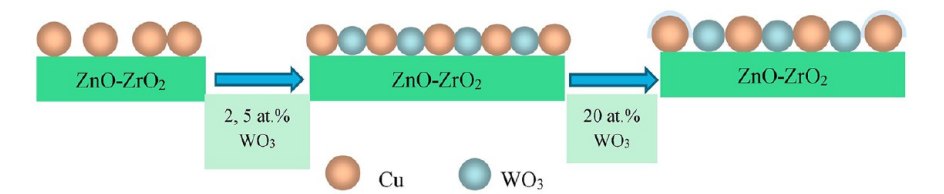


Figure 16. Graphical representation of the addition of WO_3 to a $CuO-ZnO-ZrO_2$ catalyst. Reprinted with permission from ref 128. Copyright 2018 Elsevier.

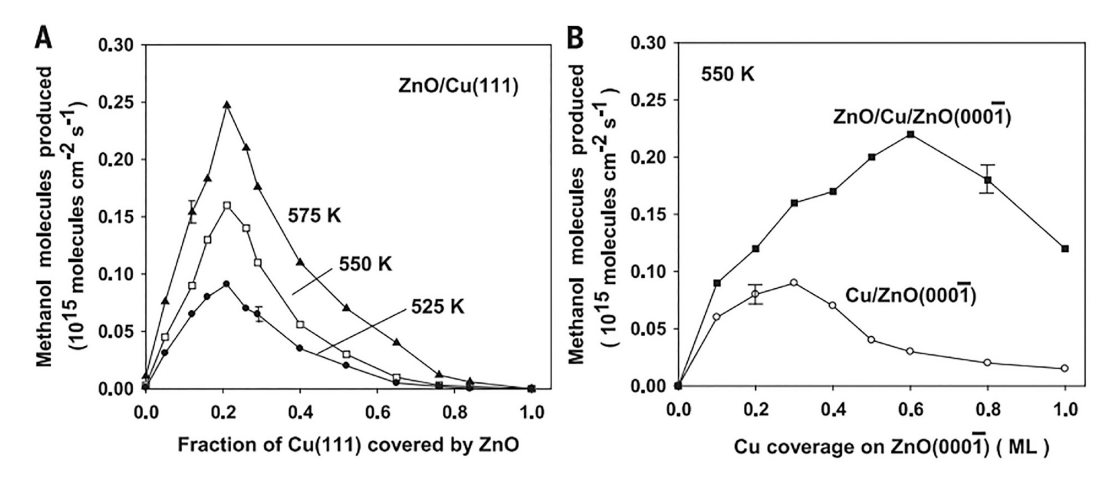


Figure 17. Methanol production rate on (A) Cu(111) as a function of the fractional surface coverage by ZnO and (B) $Cu/ZnO(000\overline{1})$ (bottom trace) and after deposition of 0.4 ML of ZnO on the $Cu/ZnO(000\overline{1})$ surface (top trace). Reprinted with permission from ref 147. Copyright 2017 American Association for the Advancement of Science.

selectivity were enhanced by the addition of small amounts of WO₃. The authors claimed that the addition of 2-10 wt % WO₃ increased the Cu dispersion, while high WO₃ loadings (20 wt %) significantly decreased it. As a result, the CO₂ conversion decreased from \sim 19% to \sim 5% for 2–5% and 20 wt % WO₃ loadings, respectively. A schematic illustration of the variation of the WO₃ content is presented in Figure 16. This shows that without the addition of WO3, the size of the Cu particles is larger (poorly dispersed), while the addition of 2–5 wt % WO3 reduced the size of the Cu species, rendering them smaller and finely dispersed. However, higher WO3 loadings led to the aggregation of copper species and partial coverage of the active copper sites, which resulted in lower catalytic activity. Characterization of the CuO-ZnO-ZrO₂-WO₃ catalysts by XRD, XPS, CO2-TPD, and H2 temperatureprogrammed reduction (H2-TPR) revealed that the activity was closely related to the specific surface area of metallic Cu, the amount of weak basic sites, and the reducibility of the catalyst, as all of them contributed to higher catalytic activity.

To conclude, hybrid oxide systems exploit the synergy that exists between metal oxides. The presence of lattice oxygen species in these materials and the reducibility of some of these metal oxides allow for interactions with the reactant gases and the creation of oxygen vacancies within defective sites. In addition, it has been shown that the arrangement of the oxides plays a significant role in directing the different reaction pathways and product selectivity; hence critical examination and selection of oxide—oxide pairs and their configuration are necessary to facilitate desired reactions. Finally, these materials have proven to be highly active and stable for methanol synthesis from CO₂ and could provide a competitive solution for industrial-scale applications.

5. COMPARISON BETWEEN TRADITIONAL AND INVERSE CATALYSTS

Traditional Cu-ZnO-based catalysts have been the most explored systems for CO₂ hydrogenation to methanol. Here, we begin by examining the benchmark Cu/ZnO catalyst along with its corresponding inverse analogs. Earlier studies were performed by Campbell et al. on Cu/ZnO(0001) and ZnO_x/ Cu(111) model catalysts for the conversion of CO₂-containing syngas to methanol at pressures close to the atmospheric (~2 atm), with negligible methanol formation (TOF $< 2 \times 10^{-3}$ molecules site-1 s-1) in both cases. 145 Then, Yang et al. employed experimental and theoretical methods to investigate the activity of Cu supported on ZnO(0001) for CO₂ hydrogenation to methanol, 146 obtaining better catalytic results with $Cu/ZnO(000\overline{1})$ than with the planar Cu(111) surface. However, more recently, Kattel et al. 147 claimed that the catalytic activity of Cu for methanol synthesis was markedly improved after vapor deposition of ZnO on the Cu(111) surface as compared to the most reactive copper surface reported in the literature, Cu(110). Interestingly, it was noticed that increasing the amount of ZnO deposited on the Cu substrate led to an increase in the activity up to a maximum at around 20% coverage, after which further addition led to higher coverage and decreased catalytic activity (Figure 17A). Although the pristine ZnO(0001) surface exhibited no catalytic activity (Figure 17B), depositing Cu on ZnO(0001) resulted in some activity for CO₂ hydrogenation (Figure 17B). However, this activity was further improved by deposition of ZnO onto the $Cu/ZnO(000\overline{1})$ catalyst to develop an inverted $ZnO/Cu/ZnO(000\overline{1})$ nanostructure (Figure 17B). These findings are representative of the formate reaction pathway that benefits from the ZnO-Cu interfacial sites.







Figure 18. Different Cu–ZnO interfaces observed on reduced Cu-ZnO-based catalysts: (a, b) interface constituted by Cu–ZnO direct contact (S1) and interface constituted by Cu (on ZnO) covered by migrated ZnO_x (S2); (c) S1 + S2 + interface constituted by isolated Cu nanoparticles covered by migrated ZnO_x (S3). Approximately 2nO Elsevier.

In another study, Wen et al. investigated the activity of both direct contact Cu-ZnO and ZnO_x-Cu NP-ZnO (via SMSI) interfaces for the RWGS reaction. 148 To do so, they synthesized a series of Cu-doped ZnO plate model catalysts via a hydrothermal route to obtain direct contact between Cu and ZnO. Additionally, they prepared a series of Cu/ZnO plate supported catalysts by wet impregnation, and these materials exhibited SMSI effect by which ZnO from the support migrates onto the Cu surface creating a ZnO_r-Cu NP-ZnO interface (in addition to the existing direct contact Cu–ZnO interface). Interestingly, supported Cu/ZnO catalysts displayed better performance than the Cu-doped ZnO model catalysts at 450 °C; however, as the temperature was increased above 500 °C, the activity of the Cu-doped catalysts was far superior to that of the supported catalysts, likely due to the increased stability of these materials at high temperatures. As the hydrogenation of CO₂ to methanol is typically performed at 250-300 °C, it is expected that the ZnO_x-Cu NP-ZnO interfacial sites play an important role in the catalytic activity. The same research group investigated the active sites on the Cu/ZnO plate supported catalysts for CO₂ hydrogenation to methanol. 149 The plate-like ZnO morphology contains a high abundance of oxygen vacancies owing to the exposure of the (002) polar facet. Based on the reduction profiles (H₂-TPR) obtained with the samples containing different Cu loadings, three different interfaces were identified, as shown in Figure 18: direct contact between Cu and ZnO plate (Cu-ZnO) (S1), migrated ZnO_x overcoating the supported Cu nanoparticles (S2), and the interface formed by migrated ZnO_x onto isolated Cu nanoparticles (S3). Then, among the different interfacial

sites, they concluded that the interfaces formed by $\rm ZnO_x$ -covered Cu (S2 and S3 in Figure 18) should have high reactivity for $\rm CO_2$ conversion and methanol production.

Le Valant et al. also studied the Cu-ZnO synergy to properly elucidate the active sites for methanol synthesis using different catalyst designs. ¹⁵⁰ In this study, they observed that a core-shell structured Cu@ZnOx catalyst, in which a ZnOx shell was grown around the Cu nanoparticles, displayed a superior methanol production rate of 4.6 mol_{MeOH} h⁻¹ kg⁻¹ (250 °C, 30 bar, and H₂/CO₂ ratio of 3) compared to other designs, such as co-precipitated Cu-ZnO (1.6 mol_{MeOH} h⁻¹ kg⁻¹, mainly producing CO via RWGS) or the mechanically mixed Cu + ZnO catalyst framework (1.4 $mol_{MeOH} h^{-1} kg^{-1}$). It was suggested that the ZnO_x shell possessed oxygen vacancies that provided the active sites necessary for methanol production. Those oxygen vacancies are generated by ZnO_x migration to the surface of the Cu nanoparticles, which facilitates the dissociative adsorption of hydrogen. As previously introduced, Palomino et al. also studied the effect of the Cu morphology on the performance of inverse ZnO/Cu catalysts. 119 To do so, they examined the behavior of ZnO/ Cu(111) and ZnO/Cu(100) catalysts for the methanol synthesis from CO₂. To synthesize those materials, Zn was deposited on Cu(111) and Cu(100) substrates in an atmosphere of O₂ at 600 K to form ZnO/CuO_x/Cu(111) and $ZnO_r/CuO_r/Cu(100)$, followed by the exposure to H_2 to obtain ZnO/Cu(111) and ZnO/Cu(100), respectively. In preliminary studies, they observed that the rate of formation of CO was 2-3 orders of magnitude higher than that for methanol over Cu(111) and Cu(100) surfaces. However, it

was noticed that the ZnO/Cu(100) catalyst displayed a higher activity for methanol synthesis than the ZnO/Cu(111) catalyst (Figure 9), with a volcano-type curve with a maximum at a relatively low coverage of 20%. At these low coverages, there probably exist small mono- and bilayer structures of ZnO on top of the copper substrates, while there is a loss of such interfacial sites at higher coverages. In addition, the improved activity of ZnO/Cu(100) as compared to the ZnO/Cu(111) catalyst proved that the morphology of the Cu substrate also affects the catalytic performance of the oxide-metal interface. The higher activity on the Cu(100) facets when compared to Cu(111) stems from the fact that the Cu(100) is more active for CO₂ dissociation. 151 AP-XPS studies on the interaction of CO₂ with Cu substrates revealed the presence of a very small coverage of atomic oxygen and adsorbed $\mathrm{CO_2}^{\delta-}$ species on Cu(111), while substantial coverage of atomic oxygen with no $CO_2^{\delta-}$ species was observed for Cu(100). Ultimately, the presence of ZnO-Cu interfacial sites favors the CO₂ binding to form formate intermediate species. The Arrhenius plot depicted in Figure 19 shows that the deposition of ZnO on

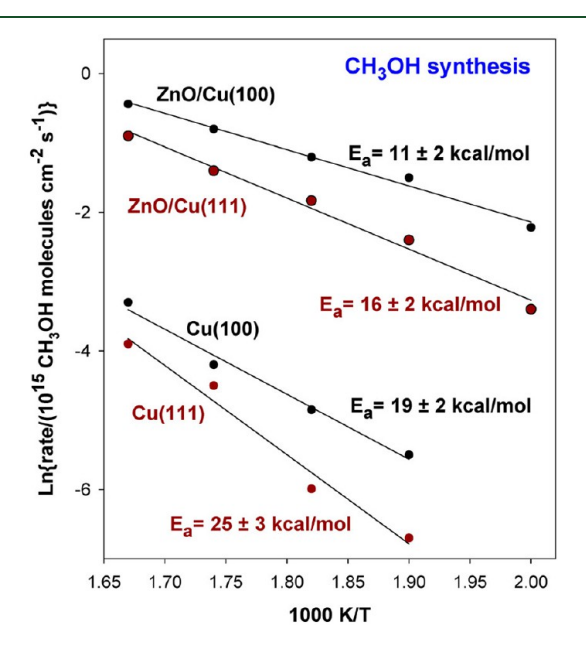


Figure 19. Arrhenius plot for CO_2 hydrogenation to methanol on plain Cu(111), Cu(100), and the Cu substrates covered with 0.2 ML of ZnO_x . Reprinted with permission from ref 119. Copyright 2018 American Chemical Society.

Cu(100) led to a decrease in the activation energy from 19 to 11 kcal/mol, with a rate of formation of methanol 15–45 times higher than that with Cu(100) within the range of investigated temperatures (500–600 K). Additionally, it can be clearly seen that ZnO/Cu(100) is much more active than ZnO/Cu(111).

As previously stated, Cu–ceria-based catalysts have also attracted significant interest for CO₂ conversion. Ouyang et al. investigated the effect of the morphology of the ceria support on Cu/CeO₂ catalysts for the hydrogenation of CO₂ to methanol. Owing to the fact that the morphology of the support plays an important role in the activity and selectivity for methanol, three different ceria structures (nanorods, nanocubes, and nanoparticles) were studied. These ceria supports were synthesized via a controlled hydrolysis method, after which the corresponding CuO/CeO₂ catalysts were

prepared by incipient wetness impregnation. The shape of the CeO₂ particles was controlled by varying the hydrothermal temperature, this being 100 °C for nanorods, 180 °C for nanocubes, and 100 °C with the addition of KOH for nanoparticles. They observed that the Cu/CeO₂ nanorod catalyst exhibited the best catalytic performance, with a methanol yield of 1.9% at 240 °C and 2 MPa, due to the strongest interaction between CuO and CeO2 and the highest CuO dispersion. The synthesized ceria nanorods were characterized by small particle sizes with exposed low index (100) and (110) facets, and the Cu precursor was reported to preferentially interact with the (110) surface that is only present on the ceria nanorods, which could have contributed to the enhanced activity. Conversely, as previously shown in Figure 7, Graciani et al. synthesized a highly active inverse CeO_x/Cu catalyst for methanol synthesis from CO_2 . In that case, 20% of the Cu substrate was covered by ceria, and the rate of formation of methanol over this catalyst was observed to be ~200 times higher than that of pristine Cu(111) and ~14 times faster than that reported with a $Cu/ZnO(000\overline{1})$ catalyst in a parallel study.¹⁰¹ They concluded that the Cuceria interface activated CO2 in the form of an unstable carboxylate $(CO_2^{\delta-})$ species, which produces methanol more easily than through the formate pathway, opening a new interesting reaction mechanism. Senanayake et al. also investigated the role of the oxide-metal interface on a CeO_x/Cu(111) catalyst for the hydrogenation of CO₂ to methanol. 113 Using AP-XPS and ambient-pressure infrared reflection absorption spectroscopy (AP-IRRAS), it was observed that both formate and carboxylate species were present during the reaction. However, it was observed that the material was rich in Ce^{3+} , which stabilizes the $CO_2^{\delta-}$ intermediate species that is essential to facilitate the formation of methanol. In this case, CeOx/Cu and ZnO/Cu inverse catalysts exhibited superior performance than the traditional supported catalysts, as shown in Figure 20. Therefore, they concluded that the addition of metal oxides onto metal

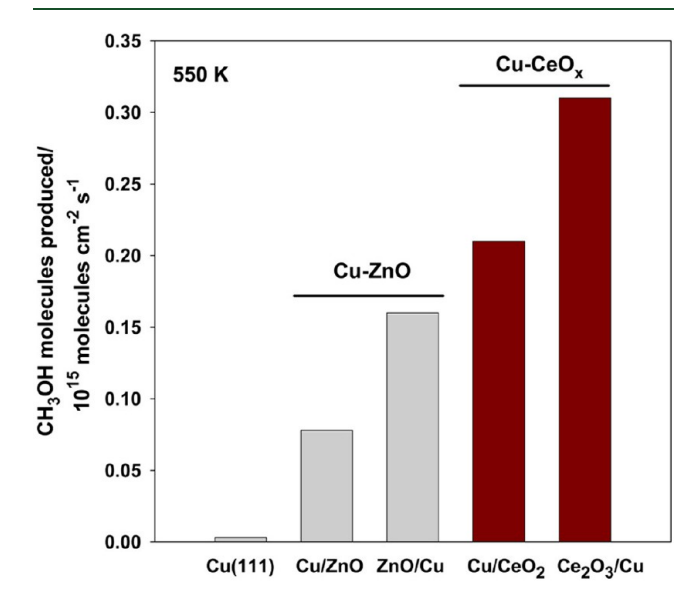


Figure 20. Rate of methanol formation over Cu(111), Cu/ZnO, Cu/CeO_2 , and inverse CeO_x/Cu and ZnO/Cu catalysts. ¹¹³ Reprinted with permission from ref 113. Copyright 2016 American Chemical Society.

surfaces (inverse catalysts) produces stronger metal—oxide interactions than when metal nanoparticles are supported on bulk oxides owing to the intrinsic nature and low reactivity of oxide supports.

It should be noted that although inverse catalyst systems have been gaining traction in recent years, not much work has focused on the use of these inverted structures for CO_2 hydrogenation. ZnO_x - and CeO_x -based inverse catalysts are two of the systems that have been more extensively studied and served as the basis of comparison in this section. However, we anticipate that the reported success of inverse catalysts will trigger more investigations in this area to yield promising results in the quest to activate and convert CO_2 into desirable products. Insights derived from these model catalysts can also serve as a blueprint for the synthesis of more practical catalysts, and the focus should be put on developing inverted structures on high-surface-area supports that can be used industrially.

6. CHALLENGES AND PERSPECTIVES

In this review, we discussed the recent advances in the development of inverse catalysts for the hydrogenation of CO₂ to methanol. We began with a brief summary of the methods used to synthesize inverted catalytic structures, particularly focusing on the challenges and opportunities available through the different synthesis routes. These synthesis methods included encapsulation approaches (such as ALD, SMSI, and core-shell techniques), newer strategies such as CSR or microemulsions, and approaches for the preparation of modelbased catalysts. As mass transfer limitations could potentially limit the performance of overcoated and core-shell catalysts, these techniques have been less frequently used to synthesize catalysts for CO₂ conversion. On the other hand, while ALD is known to create thin conformal layers with less likely mass transfer challenges, the major drawback is associated with its high cost. The extensive use of vacuum and relatively high temperatures requires very specialized equipment, which could result in expensive syntheses. 153 ALD also requires the use of high-purity substrates and precursors 154 and suffers from slow deposition rates, with most rates typically being within 100-300 nm·h⁻¹, 155 which makes scaling up also challenging. However, recently, Luterbacher and co-workers reported a liquid-based ALD process to coat a Cu catalyst with Al₂O₃ at room temperature with stoichiometric quantities of metallic precursors. As a result, this novel approach has potential to allow for scale up in more conventional commercial reactors. Further research to explore the utilization of the liquid-based ALD process to deposit oxides such as ZnO, ZrO₂, and CeO_r relevant to CO₂ hydrogenation is warranted. In the case of SMSI, there still remains a lack of clarity in the fundamental understanding of the nature of the active sites and interfacial interaction between the metal and support.²⁹ This is partly because surface reconstruction can occur under practical reaction conditions, 158 which could lead to changes in the structure of the active sites, thus making ex-situ characterization techniques less representative of the catalytic surface during reaction. 159 It is also worth mentioning that other newer approaches for inducing SMSI behavior have been reported, such as the adsorbate-mediated strong metalsupport interaction (A-SMSI)^{160,161} and wet chemistry strong metal—support interaction (wc-SMSI).¹⁶² The A-SMSI creates a permeable oxide layer around the metallic nanoparticle, which serves as a promoter, thus improving the catalytic activity. These newer SMSI techniques combined with

advancements in material characterization and surface science will lead to even better comprehension of the SMSI behavior and the synthesis of well-defined inverse catalysts. CSR has also proven to be a promising approach for the deposition of ZrO₂ on Cu for methanol synthesis from CO₂, and this could also be used for the deposition of other metal oxides, such as ceria. On the other hand, the SEA method, which has been reported for the synthesis of highly dispersed bimetallic structures, could also be potentially used for the synthesis of inverse catalysts via oxidation of the surface alloyed structures.

This review also described the use of model catalysts involving single-crystal surfaces synthesized under UHV conditions. Because of the relevance of model catalysts for surface science studies and the elucidation of active sites and reaction intermediates, this approach has been more frequently used to generate fundamental understanding of the inverse catalysts in the hydrogenation of CO₂. However, this strategy also presents challenges due to the material and pressure gaps when compared with more practical technical catalysts. Strategies to bridge this gap involve coupling these model catalysts with UHV-high-pressure reactor systems. Although in situ and operando techniques, such as STM, AP-XPS, and AP-IRRAS, have been employed, further studies are necessary to develop model catalysts that mimic those with industrial application. However, due to the well-defined nature of model catalyst surfaces, they still remain ideal candidates for DFT calculations to provide a molecular description of the hydrogenation of CO₂ on inverse catalysts.

The next section of this review focused on the impact of the inverse structures on the catalytic activity, highlighting the presence and consumption of relevant reaction intermediates. Next, the interfacial interaction and the synergistic effects between these oxides and the metal surface were reviewed in relation to the improved activity and selectivity of these materials. Following these observations, we also elaborated on hybrid oxide catalysts, a class of materials containing interfaces with similar behavior as the inverse oxide/metal catalysts. For example, In_2O_3 -based hybrid catalysts have shown to be the most promising materials in this category, with a reported methanol selectivity of nearly 100%, although relatively low CO_2 conversion under moderate reaction conditions.

Lastly, we performed a comparative evaluation of traditional oxide-supported catalysts relative to inverse structures by examining reported Cu-ZnO- and Cu-CeO_x -based materials. These comparisons showed that oxide/metal inverted structures exhibited superior performance than traditional metal/oxide catalysts for CO_2 hydrogenation. Therefore, further studies on the development and the application of practical inverse catalysts for CO_2 valorization will be necessary.

7. CONCLUSIONS

Overall, our review suggests that the development of inverse catalysts provides promising avenues for catalytic CO_2 conversion and valorization. Since the development of inverse catalysts for CO_2 conversion still appears to be at an early stage, potential future efforts should be geared toward optimizing and improving the synthesis techniques, such as those based on controlled surface reactions, microemulsions, and chemical dealloying. In addition, it is necessary to develop simpler synthesis procedures to allow for easier scale-up and large-scale production. Such process optimizations can provide opportunities for industrial implementation of such CO_2

abatement technologies. Additionally, although this inverse catalyst strategy has been primarily discussed for ${\rm CO_2}$ hydrogenation, there is a potential to extend the use of these materials to other hydrogenation reactions or other chemistries that could benefit from an increased number of metal—oxide interfacial sites.

AUTHOR INFORMATION

Corresponding Author

Ana C. Alba-Rubio — Department of Chemical Engineering, The University of Toledo, Toledo, Ohio 43606, United States; Present Address: Department of Chemical and Biomolecular Engineering, Clemson University, Clemson, SC 29634, United States.; orcid.org/0000-0002-1831-8338; Email: aalbaru@clemson.edu

Authors

Kashala Fabrice Kapiamba — Department of Chemical Engineering, The University of Toledo, Toledo, Ohio 43606, United States; Present Address: Department of Chemical, Environmental, and Materials Engineering, University of Miami, Miami, FL 33146, United States; Occid.org/0000-0003-4958-357X

Hope O. Otor — Department of Chemical Engineering, The University of Toledo, Toledo, Ohio 43606, United States; Present Address: Department of Chemical and Biomolecular Engineering, University of Notre Dame, Notre Dame, IN 46556, United States.

Sridhar Viamajala — Department of Chemical Engineering, The University of Toledo, Toledo, Ohio 43606, United States; orcid.org/0000-0003-3131-7847

Complete contact information is available at: https://pubs.acs.org/10.1021/acs.energyfuels.2c02131

Author Contributions

 $^{
m V}$ K.F.K. and H.O.O. made equal contributions.

Notes

The authors declare no competing financial interest.

Biographies

Kashala Fabrice Kapiamba received his bachelor's degree in chemical engineering from the Cape Peninsula University of Technology, South Africa, and his M.S. degree from the University of Toledo. Currently, he is a Ph.D. candidate in the Department of Chemical, Environmental, and Materials Engineering at the University of Miami. He is focused on the physical, chemical, and toxicological properties of e-cigarette aerosols. In addition, he has strong interests in air quality, climate change, and renewable energy.

Hope Otor obtained his bachelor's degree in chemical engineering from the Federal University of Technology, Minna, Nigeria, and a master's degree in chemical engineering at the University of Toledo under the supervision of Prof. Ana C. Alba-Rubio. Hope is currently a Ph.D. student in the Department of Chemical and Biomolecular Engineering at the University of Notre Dame. His primary research interests are in catalytic systems and sustainable energy applications.

Sridhar Viamajala is a professor in the Dept. of Chemical Engineering at the University of Toledo. He has B.S. and Ph.D. degrees in chemical engineering from the Indian Institute of Technology and Washington State University. He has >40 scientific publications in high quality peer-reviewed journals, is an inventor or co-inventor on 10 patent applications, and has a robust research program funded by federal and state agencies. His primary interest is in bioprocessing for the production of algal biofuels.

Ana C. Alba-Rubio is an associate professor in the Dept. of Chemical and Biomolecular Engineering at Clemson University. She has a B.S. degree in chemical engineering from the University of Málaga and a Ph.D. degree in applied physical chemistry from the Autonomous University of Madrid. Her current research interests involve the rational design and synthesis of heterogeneous catalysts to provide fuels and materials sustainably and the development of nanomaterials for sensing applications.

ACKNOWLEDGMENTS

This work was supported by the National Science Foundation under Grant No. 1847391 (now No. 2154386). Authors are also thankful to G. Alba for the design of the graphical abstract.

REFERENCES

- (1) Markewitz, P.; Kuckshinrichs, W.; Leitner, W.; Linssen, J.; Zapp, P.; Bongartz, R.; Schreiber, A.; Müller, T. E. Worldwide innovations in the development of carbon capture technologies and the utilization of CO₂. *Energy Environ. Sci.* **2012**, *5* (6), 7281–7305.
- (2) Gupta, M.; Smith, M. L.; Spivey, J. J. Heterogeneous Catalytic Conversion of Dry Syngas to Ethanol and Higher Alcohols on Cu-Based Catalysts. *ACS Catal.* **2011**, *1* (6), 641–656.
- (3) Kunduraci, M. Dealloying technique in the synthesis of lithiumion battery anode materials. *J. Solid State Electrochem.* **2016**, 20 (8), 2105–2111.
- (4) Al-Mamoori, A.; Rownaghi, A. A.; Rezaei, F. Combined Capture and Utilization of CO₂ for Syngas Production over Dual-Function Materials. ACS Sustainable Chem. Eng. 2018, 6 (10), 13551–13561.
- (5) Makuve, N.; Mehlana, G.; Tia, R.; Darkwa, J.; Makhubela, B. C. E. Hydrogenation of carbon dioxide to formate by α -diimine RuII, RhIII, IrIII complexes as catalyst precursors. *J. Organomet. Chem.* **2019**, 899, 120892.
- (6) Aresta, M.; Dibenedetto, A. The contribution of the utilization option to reducing the CO_2 atmospheric loading: research needed to overcome existing barriers for a full exploitation of the potential of the CO_2 use. *Catal. Today* **2004**, *98* (4), 455–462.
- (7) Song, C. Global challenges and strategies for control, conversion and utilization of CO_2 for sustainable development involving energy, catalysis, adsorption and chemical processing. *Catal. Today* **2006**, *115* (1–4), 2–32.
- (8) Daza, Y. A.; Kuhn, J. N. CO₂ conversion by reverse water gas shift catalysis: comparison of catalysts, mechanisms and their consequences for CO₂ conversion to liquid fuels. *RSC Adv.* **2016**, 6 (55), 49675–49691.
- (9) Luk, H. T.; Mondelli, C.; Ferre, D. C.; Stewart, J. A.; Perez-Ramirez, J. Status and prospects in higher alcohols synthesis from syngas. *Chem. Soc. Rev.* **2017**, *46* (5), 1358–1426.
- (10) Wang, J.; Zhang, G.; Zhu, J.; Zhang, X.; Ding, F.; Zhang, A.; Guo, X.; Song, C. CO₂ Hydrogenation to Methanol over In₂O₃-Based Catalysts: From Mechanism to Catalyst Development. *ACS Catal.* **2021**, *11* (3), 1406–1423.
- (11) Murthy, P. S.; Wang, Z.; Wang, L.; Zhao, J.; Wang, Z.; Liang, W.; Huang, J. Improved CO₂ Hydrogenation on Ni-ZnO/MCM-41 Catalysts with Cooperative Ni and ZnO Sites. *Energy Fuels* **2020**, 34 (12), 16320–16329.
- (12) Wei, W.; Jinlong, G. Methanation of carbon dioxide: an overview. Front. Chem. Sci. Eng. 2011, 5 (1), 2–10.
- (13) Frontera, P.; Macario, A.; Ferraro, M.; Antonucci, P. Supported Catalysts for CO₂ Methanation: A Review. *Catalysts* **2017**, *7* (2), 59. (14) Yang, Y.; Zhang, J.; Liu, J.; Wu, D.; Xiong, B.; Yang, Y.; Hua, Z. Nickel Nanoparticles Encapsulated in SSZ-13 Cage for Highly Efficient CO₂ Hydrogenation. *Energy Fuels* **2021**, 35 (16), 13240—
- (15) Younas, M.; Loong Kong, L.; Bashir, M. J. K.; Nadeem, H.; Shehzad, A.; Sethupathi, S. Recent Advancements, Fundamental Challenges, and Opportunities in Catalytic Methanation of CO₂. *Energy Fuels* **2016**, *30* (11), 8815–8831.

- (16) Esa, Y. A. M.; Sapawe, N. A short review on carbon dioxide (CO₂) methanation process. *Mater. Today: Proc.* **2020**, *31*, 394–397.
- (17) Omodolor, I. S.; Otor, H. O.; Andonegui, J. A.; Allen, B. J.; Alba-Rubio, A. C. Dual-Function Materials for CO₂ Capture and Conversion: A Review. *Ind. Eng. Chem. Res.* **2020**, *59* (40), 17612–17631.
- (18) Allison, J. N.; GoddardIII, W. A. Oxidative Dehydrogenation of Methanol to Formaldehyde. *J. Catal.* **1985**, *92*, 127–135.
- (19) Collignon, F.; Mariani, M.; Moreno, S.; Remy, M.; Poncelet, G. Gas Phase Synthesis of MTBE from Methanol and Isobutene over Dealuminated Zeolites. *J. Catal.* **1997**, *166*, 53–66.
- (20) Waters, T.; O'Hair, R. A. J.; Wedd, A. G. Catalytic Gas Phase Oxidation of Methanol to Formaldehyde. *J. Am. Chem. Soc.* **2003**, *125* (11), 3384–3396.
- (21) Miguel, C. V.; Soria, M. A.; Mendes, A.; Madeira, L. M. Direct CO2 hydrogenation to methane or methanol from post-combustion exhaust streams A thermodynamic study. *J. Nat. Gas Sci. Eng.* **2015**, 22, 1–8.
- (22) Jalama, K. Carbon dioxide hydrogenation over nickel-, ruthenium-, and copper-based catalysts: Review of kinetics and mechanism. *Catal. Rev. Sci. Eng.* **2017**, *59* (2), 95–164.
- (23) Ma, J.; Sun, N.; Zhang, X.; Zhao, N.; Xiao, F.; Wei, W.; Sun, Y. A short review of catalysis for CO₂ conversion. *Catal. Today* **2009**, 148 (3–4), 221–231.
- (24) Murthy, P. S.; Liang, W.; Jiang, Y.; Huang, J. Cu-Based Nanocatalysts for CO₂ Hydrogenation to Methanol. *Energy Fuels* **2021**, 35 (10), 8558–8584.
- (25) Rodríguez, J. A.; Hrbek, J. Inverse oxide/metal catalysts: A versatile approach for activity tests and mechanistic studies. *Surf. Sci.* **2010**, *604* (3–4), 241–244.
- (26) Reuel, R. C.; Bartholomew, C. H. Effects of support and dispersion on the CO hydrogenation activity/selectivity properties of cobalt. *J. Catal.* **1984**, *85*, 78–88.
- (27) Zhang, J.; Medlin, J. W. Catalyst design using an inverse strategy: From mechanistic studies on inverted model catalysts to applications of oxide-coated metal nanoparticles. *Surf. Sci. Rep.* **2018**, 73 (4), 117–152.
- (28) Orozco, I.; Huang, E.; Mahapatra, M.; Kang, J.; Shi, R.; Nemšák, S.; Tong, X.; Senanayake, S. D.; Liu, P.; Rodríguez, J. A. Understanding Methanol Synthesis on Inverse ZnO/CuO_x/Cu Catalysts: Stability of CH₃O Species and Dynamic Nature of the Surface. *J. Phys. Chem. C* **2021**, *125* (12), 6673–6683.
- (29) Wu, C.; Cheng, D.; Wang, M.; Ma, D. Understanding and Application of Strong Metal-Support Interactions in Conversion of CO₂ to Methanol: A Review. *Energy Fuels* **2021**, *35* (23), 19012–19023.
- (30) Shen, C.; Bao, Q.; Xue, W.; Sun, K.; Zhang, Z.; Jia, X.; Mei, D.; Liu, C.-j. Synergistic effect of the metal-support interaction and interfacial oxygen vacancy for CO_2 hydrogenation to methanol over Ni/In_2O_3 catalyst: A theoretical study. *J. Energy Chem.* **2022**, *65*, *623*–*629*.
- (31) Schoiswohl, J.; Surnev, S.; Netzer, F. P. Reactions on Inverse Model Catalyst Surfaces: Atomic Views by STM. *Top. Catal.* **2005**, *36* (1–4), 91–105.
- (32) Rodriguez, J. A.; Liu, P.; Graciani, J.; Senanayake, S. D.; Grinter, D. C.; Stacchiola, D.; Hrbek, J.; Fernandez-Sanz, J. Inverse Oxide/Metal Catalysts in Fundamental Studies and Practical Applications: A Perspective of Recent Developments. *J. Phys. Chem. Lett.* **2016**, 7 (13), 2627–39.
- (33) Kang, J.; Rui, N.; Huang, E.; Tian, Y.; Mahapatra, M.; Rosales, R.; Orozco, I.; Shi, R.; Senanayake, S. D.; Liu, P.; Rodriguez, J. A. Surface characterization and methane activation on $SnO_x/Cu_2O/Cu(111)$ inverse oxide/metal catalysts. *Phys. Chem. Chem. Phys.* **2021**, 23 (32), 17186–17196.
- (34) Wu, Q.; Liang, S.; Zhang, T.; Louis, B.; Wang, Q. Current advances in bimetallic catalysts for carbon dioxide hydrogenation to methanol. *Fuel* **2022**, *313*, 122963.
- (35) Kanuri, S.; Roy, S.; Chakraborty, C.; Datta, S. P.; Singh, S. A.; Dinda, S. An insight of CO₂ hydrogenation to methanol synthesis:

- Thermodynamics, catalysts, operating parameters, and reaction mechanism. *Int. J. Energy Res.* **2022**, *46* (5), 5503–5522.
- (36) Meng, X.-Y.; Peng, C.; Jia, J.; Liu, P.; Men, Y.-L.; Pan, Y.-X. Recent progress and understanding on In₂O₃-based composite catalysts for boosting CO₂ hydrogenation. *J. CO2 Util.* **2022**, *55*, 101844.
- (37) Niu, J.; Liu, H.; Jin, Y.; Fan, B.; Qi, W.; Ran, J. Comprehensive review of Cu-based CO₂ hydrogenation to CH₃OH: Insights from experimental work and theoretical analysis. *Int. J. Hydrogen Energy* **2022**, *47* (15), 9183–9200.
- (38) Bai, S. T.; De Smet, G.; Liao, Y.; Sun, R.; Zhou, C.; Beller, M.; Maes, B. U. W.; Sels, B. F. Homogeneous and heterogeneous catalysts for hydrogenation of CO₂ to methanol under mild conditions. *Chem. Soc. Rev.* **2021**, *50* (7), 4259–4298.
- (39) Saeidi, S.; Najari, S.; Hessel, V.; Wilson, K.; Keil, F. J.; Concepción, P.; Suib, S. L.; Rodrigues, A. E. Recent advances in CO₂ hydrogenation to value-added products Current challenges and future directions. *Prog. Energy Combust. Sci.* **2021**, *85*, 100905.
- (40) Atsbha, T. A.; Yoon, T.; Seongho, P.; Lee, C.-J. A review on the catalytic conversion of CO_2 using H_2 for synthesis of CO_3 methanol, and hydrocarbons. *J. CO2 Util.* **2021**, *44*, 101413.
- (41) Ra, E. C.; Kim, K. Y.; Kim, E. H.; Lee, H.; An, K.; Lee, J. S. Recycling Carbon Dioxide through Catalytic Hydrogenation: Recent Key Developments and Perspectives. *ACS Catal.* **2020**, *10* (19), 11318–11345.
- (42) Jiang, X.; Nie, X.; Guo, X.; Song, C.; Chen, J. G. Recent Advances in Carbon Dioxide Hydrogenation to Methanol via Heterogeneous Catalysis. *Chem. Rev.* **2020**, *120* (15), 7984–8034.
- (43) Chang, K.; Zhang, H.; Cheng, M.-j.; Lu, Q. Application of Ceria in CO₂ Conversion Catalysis. ACS Catal. 2020, 10 (1), 613–631.
- (44) Furimsky, E. CO₂ Hydrogenation to Methanol and Methane over Carbon-Supported Catalysts. *Ind. Eng. Chem. Res.* **2020**, 59 (35), 15393–15423.
- (45) Gao, P.; Zhang, L.; Li, S.; Zhou, Z.; Sun, Y. Novel Heterogeneous Catalysts for CO₂ Hydrogenation to Liquid Fuels. *ACS Cent Sci.* **2020**, *6* (10), 1657–1670.
- (46) Zhong, J.; Yang, X.; Wu, Z.; Liang, B.; Huang, Y.; Zhang, T. State of the art and perspectives in heterogeneous catalysis of CO_2 hydrogenation to methanol. *Chem. Soc. Rev.* **2020**, 49 (5), 1385–1413.
- (47) Xie, S.; Zhang, W.; Lan, X.; Lin, H. CO₂ Reduction to Methanol in the Liquid Phase: A Review. *ChemSusChem* **2020**, *13* (23), 6141–6159.
- (48) Sha, F.; Han, Z.; Tang, S.; Wang, J.; Li, C. Hydrogenation of Carbon Dioxide to Methanol over Non-Cu-based Heterogeneous Catalysts. *ChemSusChem* **2020**, *13* (23), 6160–6181.
- (49) Gao, X.; Atchimarungsri, T.; Ma, Q.; Zhao, T.-S.; Tsubaki, N. Realizing efficient carbon dioxide hydrogenation to liquid hydrocarbons by tandem catalysis design. *EnergyChem.* **2020**, *2* (4), 100038.
- (50) Li, K.; Chen, J. G. CO₂ Hydrogenation to Methanol over ZrO₂-Containing Catalysts: Insights into ZrO₂ Induced Synergy. *ACS Catal.* **2019**, *9* (9), 7840–7861.
- (51) Tosoni, S.; Pacchioni, G. Oxide-Supported Gold Clusters and Nanoparticles in Catalysis: A Computational Chemistry Perspective. *ChemCatChem.* **2019**, *11* (1), 73–89.
- (52) Din, I. U.; Shaharun, M. S.; Alotaibi, M. A.; Alharthi, A. I.; Naeem, A. Recent developments on heterogeneous catalytic CO₂ reduction to methanol. *J. CO2 Util.* **2019**, *34*, 20–33.
- (53) Masui, T.; Fujiwara, K.; Machida, K.-i.; Adachi, G.-y.; Sakata, T.; Mori, H. Characterization of Cerium(IV) Oxide Ultrafine Particles Prepared Using Reversed Micelles. *Chem. Mater.* **1997**, 9 (10), 2197–2204.
- (54) Eriksson, S. Preparation of catalysts from microemulsions and their applications in heterogeneous catalysis. *Appl. Catal. A-Gen.* **2004**, 265 (2), 207–219.
- (55) Zhao, G.; Wu, X. P.; Chai, R.; Zhang, Q.; Gong, X. Q.; Huang, J.; Lu, Y. Tailoring nano-catalysts: turning gold nanoparticles on bulk metal oxides to inverse nano-metal oxides on large gold particles. *Chem. Commun. (Camb)* **2015**, *51* (27), 5975–8.

- (56) Yao, Q.; Wang, C.; Wang, H.; Yan, H.; Lu, J. Revisiting the Au Particle Size Effect on TiO₂-Coated Au/TiO₂ Catalysts in CO Oxidation Reaction. *J. Phys. Chem. C* **2016**, *120* (17), 9174–9183.
- (57) Lee, S. W.; Song, J. T.; Kim, J.; Oh, J.; Park, J. Y. Enhanced catalytic activity for CO oxidation by the metal-oxide perimeter of $\text{TiO}_2/\text{nanostructured}$ Au inverse catalysts. *Nanoscale* **2018**, *10* (8), 3911–3917.
- (58) Qadir, K.; Quynh, B. T.; Lee, H.; Moon, S. Y.; Kim, S. H.; Park, J. Y. Tailoring metal-oxide interfaces of inverse catalysts of TiO₂/nanoporous-Au under hydrogen oxidation. *Chem. Commun.* (Camb) **2015**, *51* (47), 9620–3.
- (59) Lee, S. W.; Lee, C.; Goddeti, K. C.; Kim, S. M.; Park, J. Y. Surface plasmon-driven catalytic reactions on a patterned Co₃O₄/Au inverse catalyst. *RSC Adv.* **2017**, *7* (88), 56073–56080.
- (60) Lunkenbein, T.; Schumann, J.; Behrens, M.; Schlogl, R.; Willinger, M. G. Formation of a ZnO overlayer in industrial Cu/ZnO/Al₂O₃ catalysts induced by strong metal-support interactions. *Angew. Chem., Int. Ed. Engl.* **2015**, *54* (15), 4544–8.
- (61) Shen, Y.; Xiao, Z.; Liu, J.; Wang, Z. Facile Preparation of Inverse Nanoporous Cr₂O₃/Cu Catalysts for Reverse Water-Gas Shift Reaction. *ChemCatChem.* **2019**, *11* (22), 5439–5443.
- (62) Otor, H. O.; Steiner, J. B.; García-Sancho, C.; Alba-Rubio, A. C. Encapsulation Methods for Control of Catalyst Deactivation: A Review. ACS Catal. 2020, 10 (14), 7630–7656.
- (63) Tauster, S. J.; Fung, S. C.; Garten, R. L. Strong metal-support interactions. Group 8 noble metals supported on titanium dioxide. *J. Am. Chem. Soc.* **1978**, *100* (1), 170–175.
- (64) Tauster, S. J.; Fung, S. C. Strong metal-support interactions: occurrence among the binary oxides of groups IIA-VB. *J. Catal.* **1978**, 55 (1), 29.
- (65) Díez-Ramírez, J.; Dorado, F.; de la Osa, A. R.; Valverde, J. L.; Sánchez, P. Hydrogenation of CO₂ to Methanol at Atmospheric Pressure over Cu/ZnO Catalysts: Influence of the Calcination, Reduction, and Metal Loading. *Ind. Eng. Chem. Res.* **2017**, *56* (8), 1979–1987.
- (66) Behrens, M.; Zander, S.; Kurr, P.; Jacobsen, N.; Senker, J.; Koch, G.; Ressler, T.; Fischer, R. W.; Schlogl, R. Performance improvement of nanocatalysts by promoter-induced defects in the support material: methanol synthesis over Cu/ZnO:Al. *J. Am. Chem. Soc.* 2013, 135 (16), 6061–8.
- (67) Sneh, O.; Clark-Phelps, R. B.; Londergan, A. R.; Winkler, J.; Seidel, T. E. Thin film atomic layer deposition equipment for semiconductor processing. *Thin solid films* **2002**, 402, 248–261.
- (68) Lu, J.; Elam, J. W.; Stair, P. C. Atomic layer deposition—Sequential self-limiting surface reactions for advanced catalyst "bottom-up" synthesis. *Surf. Sci. Rep.* **2016**, 71 (2), 410–472.
- (69) Leskelä, M.; Ritala, M. Atomic layer deposition (ALD): from precursors to thin film structures. *Thin solid films* **2002**, 409 (1), 138–146.
- (70) George, S. M. Atomic Layer Deposition: An Overview. *Chem. Rev.* **2010**, *110*, 111–131.
- (71) Kim, D. W.; Kim, K.-D.; Seo, H. O.; Dey, N. K.; Kim, M. J.; Kim, Y. D.; Lim, D. C.; Lee, K. H. TiO₂/Ni Inverse-Catalysts Prepared by Atomic Layer Deposition (ALD). *Catal. Lett.* **2011**, *141* (6), 854–859.
- (72) Seo, H. O.; Sim, J. K.; Kim, K.-D.; Kim, Y. D.; Lim, D. C.; Kim, S. H. Carbon dioxide reforming of methane to synthesis gas over a TiO₂-Ni inverse catalyst. *Appl. Catal. A-Gen.* **2013**, *451*, 43–49.
- (73) Oviroh, P. O.; Akbarzadeh, R.; Pan, D.; Coetzee, R. A. M.; Jen, T. C. New development of atomic layer deposition: processes, methods and applications. *Sci. Technol. Adv. Mater.* **2019**, 20 (1), 465–496.
- (74) Cargnello, M.; Montini, T.; Polizzi, S.; Wieder, N. L.; Gorte, R. J.; Graziani, M.; Fornasiero, P. Novel embedded Pd@CeO₂ catalysts: a way to active and stable catalysts. *Dalton Trans.* **2010**, 39 (8), 2122–7.
- (75) Bakhmutsky, K.; Wieder, N. L.; Cargnello, M.; Galloway, B.; Fornasiero, P.; Gorte, R. J. A versatile route to core-shell catalysts:

- synthesis of dispersible M@oxide (M = Pd, Pt; oxide = TiO_2 , ZrO_2) nanostructures by self-assembly. ChemSusChem **2012**, 5 (1), 140–8.
- (76) Chen, C.; Shi, M.; Cargnello, M.; Fornasiero, P.; Murray, C. B.; Gorte, R. J. Au@TiO₂ Core-Shell Nanostructures with High Thermal Stability. *Catal. Lett.* **2014**, *144* (11), 1939–1945.
- (77) Forman, A. J.; Park, J.-N.; Tang, W.; Hu, Y.-S.; Stucky, G. D.; McFarland, E. W. Silica-Encapsulated Pd Nanoparticles as a Regenerable and Sintering-Resistant Catalyst. *ChemCatChem.* **2010**, 2 (10), 1318–1324.
- (78) Park, J. N.; Forman, A. J.; Tang, W.; Cheng, J.; Hu, Y. S.; Lin, H.; McFarland, E. W. Highly active and sinter-resistant Pd-nanoparticle catalysts encapsulated in silica. *Small* **2008**, *4* (10), 1694–7.
- (79) Stöber, W.; Fink, A.; Bohn, E. Controlled growth of monodisperse silica spheres in the micron size range. *J. Colloid Interface Sci.* 1968, 26 (1), 62–69.
- (80) Wang, H.; Zhang, J.-f.; Bai, Y.-x.; Wang, W.-f.; Tan, Y.-s.; Han, Y.-z. NiO@SiO₂ core-shell catalyst for low-temperature methanation of syngas in slurry reactor. *J. Fuel Chem. Technol.* **2016**, 44 (5), 548–556.
- (81) Ashik, U. P. M.; Daud, W. M. A. W. Probing the differential methane decomposition behaviors of n-Ni/SiO₂, n-Fe/SiO₂ and n-Co/SiO₂ catalysts prepared by co-precipitation cum modified Stöber method. *RSC Adv.* **2015**, *5* (82), 67227–67241.
- (82) Yang, W.; Liu, H.; Li, Y.; Zhang, J.; Wu, H.; He, D. Properties of yolk-shell structured Ni@SiO₂ nanocatalyst and its catalytic performance in carbon dioxide reforming of methane to syngas. *Catal. Today* **2016**, 259, 438–445.
- (83) Gioria, E.; Duarte-Correa, L.; Bashiri, N.; Hetaba, W.; Schomaecker, R.; Thomas, A. Rational design of tandem catalysts using a core-shell structure approach. *Nanoscale Adv.* **2021**, 3 (12), 3454–3459.
- (84) Das, S.; Kawi, S.Core-Shell Structured Catalysts for Catalytic Conversion of CO₂ to Syngas. In *Core-Shell and Yolk-Shell Nanocatalysts*; Yamashita, H., Li, H., Eds.; Springer Singapore: Singapore, 2021; pp 121–149.
- (85) Alba-Rubio, A. C.; Sener, C.; Hakim, S. H.; Gostanian, T. M.; Dumesic, J. A. Synthesis of Supported RhMo and PtMo Bimetallic Catalysts by Controlled Surface Reactions. *ChemCatChem.* **2015**, 7 (23), 3881–3886.
- (86) Sener, C.; Wesley, T. S.; Alba-Rubio, A. C.; Kumbhalkar, M. D.; Hakim, S. H.; Ribeiro, F. H.; Miller, J. T.; Dumesic, J. A. PtMo Bimetallic Catalysts Synthesized by Controlled Surface Reactions for Water Gas Shift. *ACS Catal.* **2016**, *6* (2), 1334–1344.
- (87) Ro, I.; Liu, Y.; Ball, M. R.; Jackson, D. H. K.; Chada, J. P.; Sener, C.; Kuech, T. F.; Madon, R. J.; Huber, G. W.; Dumesic, J. A. Role of the Cu-ZrO₂ Interfacial Sites for Conversion of Ethanol to Ethyl Acetate and Synthesis of Methanol from CO₂ and H₂. ACS Catal. **2016**, 6 (10), 7040–7050.
- (88) Hakim, S. H.; Sener, C.; Alba-Rubio, A. C.; Gostanian, T. M.; O'Neill, B. J.; Ribeiro, F. H.; Miller, J. T.; Dumesic, J. A. Synthesis of supported bimetallic nanoparticles with controlled size and composition distributions for active site elucidation. *J. Catal.* **2015**, 328, 75–90.
- (89) Carrasquillo-Flores, R.; Ro, I.; Kumbhalkar, M. D.; Burt, S.; Carrero, C. A.; Alba-Rubio, A. C.; Miller, J. T.; Hermans, I.; Huber, G. W.; Dumesic, J. A. Reverse Water-Gas Shift on Interfacial Sites Formed by Deposition of Oxidized Molybdenum Moieties onto Gold Nanoparticles. J. Am. Chem. Soc. 2015, 137 (32), 10317–25.
- (90) Boutonnet, M.; Sanchez-Dominguez, M. Microemulsion droplets to catalytically active nanoparticles. How the application of colloidal tools in catalysis aims to well designed and efficient catalysts. *Catal. Today* **2017**, 285, 89–103.
- (91) Sun, G.; Mottaghi-Tabar, S.; Ricardez-Sandoval, L.; Simakov, D. S. A. Highly Active, Selective and Stable Reverse Water Gas Shift Catalyst Based on High Surface Area MoC/γ -Al₂O₃ Synthesized by Reverse Microemulsion. *Top. Catal.* **2021**, *64* (5–6), 414–430.
- (92) Herranz, T.; Rojas, S.; Pérez-Alonso, F. J.; Ojeda, M.; Terreros, P.; Fierro, J. L. G. Hydrogenation of carbon oxides over promoted Fe-

- Mn catalysts prepared by the microemulsion methodology. *Appl. Catal. A-Gen.* **2006**, 311, 66–75.
- (93) Wang, G.; Luo, F.; Lin, L.; Zhao, F. Inverse ZnO/Cu catalysts for methanol synthesis from CO₂ hydrogenation. *React. Kinet.Mech. Catal.* **2021**, 132 (1), 155–170.
- (94) Gao, F.; Goodman, D. W. Model catalysts: simulating the complexities of heterogeneous catalysts. *Annu. Rev. Phys. Chem.* **2012**, 63, 265–86.
- (95) Rodriguez, J. A.; Grinter, D. C.; Liu, Z.; Palomino, R. M.; Senanayake, S. D. Ceria-based model catalysts: fundamental studies on the importance of the metal-ceria interface in CO oxidation, the water-gas shift, CO₂ hydrogenation, and methane and alcohol reforming. *Chem. Soc. Rev.* **2017**, *46* (7), 1824–1841.
- (96) Kim, M. S.; Lee, D. W.; Chung, S. H.; Hong, Y. K.; Lee, S. H.; Oh, S. H.; Cho, I. H.; Lee, K. Y. Oxidation of ammonia to nitrogen over Pt/Fe/ZSM5 catalyst: influence of catalyst support on the low temperature activity. *I. Hazard Mater.* **2012**, 237–238, 153–60.
- (97) Oemar, U.; Hidajat, K.; Kawi, S. Role of catalyst support over PdO-NiO catalysts on catalyst activity and stability for oxy-CO₂ reforming of methane. *Appl. Catal. A-Gen.* **2011**, 402 (1–2), 176–187.
- (98) Liu, S.; Wu, X.; Weng, D.; Ran, R. Ceria-based catalysts for soot oxidation: a review. *J. Rare Earths* **2015**, *33* (6), 567–590.
- (99) Trovarelli, A. Catalytic Properties of Ceria and CeO₂-Containing Materials. *Catal. Rev. Sci. Eng.* **1996**, 38 (4), 439–520.
- (100) O'Connell, M.; Morris, M. A. New ceria-based catalysts for pollution abatement. *Catal. Today* **2000**, *59*, 387–393.
- (101) Graciani, J.; Mudiyanselage, K.; Xu, F.; Baber, A. E.; Evans, J.; Senanayake, S. D.; Stacchiola, D. J.; Liu, P.; Hrbek, J.; Sanz, J. F.; Rodriguez, J. A. Highly active copper-ceria and copper-ceria-titania catalysts for methanol synthesis from CO₂. *Science* **2014**, *345*, 546–550
- (102) Avgouropoulos, G.; Papavasiliou, J.; Tabakova, T.; Idakiev, V.; Ioannides, T. A comparative study of ceria-supported gold and copper oxide catalysts for preferential CO oxidation reaction. *Chem. Eng. J.* **2006**, *124* (1–3), 41–45.
- (103) Fuchs, M.; Jenewein, B.; Penner, S.; Hayek, K.; Rupprechter, G.; Wang, D.; Schlögl, R.; Calvino, J. J.; Bernal, S. Interaction of Pt and Rh nanoparticles with ceria supports: Ring opening of methylcyclobutane and CO hydrogenation after reduction at 373—723K. Appl. Catal. A- Gen. 2005, 294 (2), 279—289.
- (104) Toyoda, T.; Nishihara, Y.; Qian, E. W. CO hydrogenation on group VI metal-ceria catalysts. *Fuel Process. Technol.* **2014**, *125*, 86–93
- (105) Wang, P.; Zhang, J.; Bai, Y.; Xiao, H.; Tian, S.; Xie, H.; Yang, G.; Tsubaki, N.; Han, Y.; Tan, Y. Ternary copper-cobalt-cerium catalyst for the production of ethanol and higher alcohols through CO hydrogenation. *Appl. Catal. A-Gen.* **2016**, *514*, 14–23.
- (106) Kiennemann, A.; Breault, R.; Hindermann, J.-P.; Laurin, M. Ethanol promotion by the addition of cerium to rhodium-silica catalysts. *J. Chem. Soc., Faraday Trans.* 1 1987, 83, 2119–2128.
- (107) Salcedo, A.; Irigoyen, B. Unraveling the Origin of Ceria Activity in Water-Gas Shift by First-Principles Microkinetic Modeling. *J. Phys. Chem. C* **2020**, *124* (14), 7823–7834.
- (108) Hu, X.; Qin, W.; Guan, Q.; Li, W. The Synergistic Effect of CuZnCeO_x in Controlling the Formation of Methanol and CO from CO₂ Hydrogenation. *ChemCatChem.* **2018**, *10* (19), 4438–4449.
- (109) Zhao, B.; Pan, Y.-x.; Liu, C.-j. The promotion effect of CeO₂ on CO₂ adsorption and hydrogenation over Ga₂O₃. *Catal. Today* **2012**, *194* (1), 60–64.
- (110) Damyanova, S.; Bueno, J. M. C. Effect of CeO₂ loading on the surface and catalytic behaviors of CeO₂-Al₂O₃-supported Pt catalysts. *Appl. Catal. A-Gen.* **2003**, 253 (1), 135–150.
- (111) Kaemena, B.; Senanayake, S. D.; Meyer, A.; Sadowski, J. T.; Falta, J.; Flege, J. I. Growth and Morphology of Ceria on Ruthenium (0001). *J. Phys. Chem. C* **2013**, *117* (1), 221–232.
- (112) Lu, J. L.; Gao, H. J.; Shaikhutdinov, S.; Freund, H. J. Morphology and defect structure of the CeO₂(111) films grown on

- Ru(0001) as studied by scanning tunneling microscopy. *Surf. Sci.* **2006**, 600 (22), 5004–5010.
- (113) Senanayake, S. D.; Ramírez, P. J.; Waluyo, I.; Kundu, S.; Mudiyanselage, K.; Liu, Z.; Liu, Z.; Axnanda, S.; Stacchiola, D. J.; Evans, J.; Rodriguez, J. A. Hydrogenation of CO_2 to Methanol on $CeO_x/Cu(111)$ and ZnO/Cu(111) Catalysts: Role of the Metal-Oxide Interface and Importance of Ce^{3+} Sites. *J. Phys. Chem. C* **2016**, 120 (3), 1778–1784.
- (114) Nakamura, J.; Fujitani, T.; Kuld, S.; Helveg, S.; Chorkendorff, I.; Sehested, J. Comment on "Active sites for CO₂ hydrogenation to methanol on Cu/ZnO catalysts". *Science* **2017**, *357*, eaan8074.
- (115) Schumann, J.; Eichelbaum, M.; Lunkenbein, T.; Thomas, N.; Álvarez Galván, M. C.; Schlögl, R.; Behrens, M. Promoting Strong Metal Support Interaction: Doping ZnO for Enhanced Activity of Cu/ZnO:M (M = Al, Ga, Mg) Catalysts. *ACS Catal.* **2015**, *5* (6), 3260–3270.
- (116) Carvalho, D. F.; Almeida, G. C.; Monteiro, R. S.; Mota, C. J. A. Hydrogenation of CO₂ to Methanol and Dimethyl Ether over a Bifunctional Cu·ZnO Catalyst Impregnated on Modified γ-Alumina. *Energy Fuels* **2020**, 34 (6), 7269–7274.
- (117) Reichenbach, T.; Mondal, K.; Jäger, M.; Vent-Schmidt, T.; Himmel, D.; Dybbert, V.; Bruix, A.; Krossing, I.; Walter, M.; Moseler, M. Ab initio study of CO₂ hydrogenation mechanisms on inverse ZnO/Cu catalysts. *J. Catal.* **2018**, *360*, 168–174.
- (118) Tisseraud, C.; Comminges, C.; Habrioux, A.; Pronier, S.; Pouilloux, Y.; Le Valant, A. Cu-ZnO catalysts for CO₂ hydrogenation to methanol: Morphology change induced by ZnO lixiviation and its impact on the active phase formation. *Mol. Catal.* **2018**, 446, 98–105.
- (119) Palomino, R. M.; Ramirez, P. J.; Liu, Z.; Hamlyn, R.; Waluyo, I.; Mahapatra, M.; Orozco, I.; Hunt, A.; Simonovis, J. P.; Senanayake, S. D.; Rodriguez, J. A. Hydrogenation of CO_2 on ZnO/Cu(100) and ZnO/Cu(111) Catalysts: Role of Copper Structure and Metal-Oxide Interface in Methanol Synthesis. *J. Phys. Chem. B* **2018**, *122* (2), 794–800.
- (120) Guil-Lopez, R.; Mota, N.; Llorente, J.; Millan, E.; Pawelec, B.; Fierro, J. L. G.; Navarro, R. M. Methanol Synthesis from CO₂: A Review of the Latest Developments in Heterogeneous Catalysis. *Materials (Basel)* **2019**, *12* (23), 3902.
- (121) Bowker, M. Methanol Synthesis from CO₂ Hydrogenation. ChemCatChem. 2019, 11 (17), 4238–4246.
- (122) Zhao, Y.-F.; Yang, Y.; Mims, C.; Peden, C. H. F.; Li, J.; Mei, D. Insight into methanol synthesis from CO₂ hydrogenation on Cu(111): Complex reaction network and the effects of H₂O. *J. Catal.* **2011**, 281 (2), 199–211.
- (123) Porosoff, M. D.; Yan, B.; Chen, J. G. Catalytic reduction of CO₂ by H₂ for synthesis of CO, methanol and hydrocarbons: challenges and opportunities. *Energy Environ. Sci.* **2016**, *9* (1), 62–73. (124) Kattel, S.; Yan, B.; Yang, Y.; Chen, J. G.; Liu, P. Optimizing Binding Energies of Key Intermediates for CO₂ Hydrogenation to Methanol over Oxide-Supported Copper. *J. Am. Chem. Soc.* **2016**, *138* (38), 12440–50.
- (125) Larmier, K.; Liao, W. C.; Tada, S.; Lam, E.; Verel, R.; Bansode, A.; Urakawa, A.; Comas-Vives, A.; Coperet, C. CO₂-to-Methanol Hydrogenation on Zirconia-Supported Copper Nanoparticles: Reaction Intermediates and the Role of the Metal-Support Interface. *Angew. Chem., Int. Ed. Engl.* **2017**, *56* (9), 2318–2323.
- (126) Witoon, T.; Chalorngtham, J.; Dumrongbunditkul, P.; Chareonpanich, M.; Limtrakul, J. CO₂ hydrogenation to methanol over Cu/ZrO₂ catalysts: Effects of zirconia phases. *Chem. Eng. J.* **2016**, 293, 327–336.
- (127) Wu, C.; Lin, L.; Liu, J.; Zhang, J.; Zhang, F.; Zhou, T.; Rui, N.; Yao, S.; Deng, Y.; Yang, F.; Xu, W.; Luo, J.; Zhao, Y.; Yan, B.; Wen, X. D.; Rodriguez, J. A.; Ma, D. Inverse ZrO₂/Cu as a highly efficient methanol synthesis catalyst from CO₂ hydrogenation. *Nat. Commun.* **2020**, *11* (1), 5767.
- (128) Wang, G.; Mao, D.; Guo, X.; Yu, J. Enhanced performance of the CuO-ZnO-ZrO₂ catalyst for CO₂ hydrogenation to methanol by WO₃ modification. *Appl. Surf. Sci.* **2018**, *456*, 403–409.

- (129) Zou, T.; Araújo, T. P.; Krumeich, F.; Mondelli, C.; Pérez-Ramírez, J. ZnO-Promoted Inverse ZrO₂-Cu Catalysts for CO₂-Based Methanol Synthesis under Mild Conditions. *ACS Sustainable Chem. Eng.* **2022**, *10* (1), 81–90.
- (130) Ma, Y.; Wang, J.; Goodman, K. R.; Head, A. R.; Tong, X.; Stacchiola, D. J.; White, M. G. Reactivity of a Zirconia-Copper Inverse Catalyst for CO₂ Hydrogenation. *J. Phys. Chem. C* **2020**, *124* (40), 22158–22172.
- (131) Hamlyn, R.; Mahapatra, M.; Orozco, I.; Hunt, A.; Waluyo, I.; White, M. G.; Senanayake, S. D.; Rodriguez, J. Morphology and chemical behavior of model $CsO_x/Cu_2O/Cu(111)$ nanocatalysts for methanol synthesis: Reaction with CO_2 and H_2 . J. Chem. Phys. **2020**, 152 (4), 044701.
- (132) Hu, B.; Yin, Y.; Zhong, Z.; Wu, D.; Liu, G.; Hong, X. Cu@ ZIF-8 derived inverse ZnO/Cu catalyst with sub-5 nm ZnO for efficient CO₂ hydrogenation to methanol. *Catal. Sci. Technol.* **2019**, 9 (10), 2673–2681.
- (133) Yang, X.; Kattel, S.; Senanayake, S. D.; Boscoboinik, J. A.; Nie, X.; Graciani, J.; Rodriguez, J. A.; Liu, P.; Stacchiola, D. J.; Chen, J. G. Low Pressure CO₂ Hydrogenation to Methanol over Gold Nanoparticles Activated on a CeO_x/TiO₂ Interface. *J. Am. Chem. Soc.* **2015**, 137 (32), 10104–7.
- (134) Konsolakis, M.; Lykaki, M. Recent Advances on the Rational Design of Non-Precious Metal Oxide Catalysts Exemplified by CuO_x/CeO₂ Binary System: Implications of Size, Shape and Electronic Effects on Intrinsic Reactivity and Metal-Support Interactions. *Catalysts* **2020**, *10* (2), 160.
- (135) Li, C. S.; Melaet, G.; Ralston, W. T.; An, K.; Brooks, C.; Ye, Y.; Liu, Y. S.; Zhu, J.; Guo, J.; Alayoglu, S.; Somorjai, G. A. Highperformance hybrid oxide catalyst of manganese and cobalt for low-pressure methanol synthesis. *Nat. Commun.* **2015**, *6*, 6538.
- (136) Frei, M. S.; Mondelli, C.; Cesarini, A.; Krumeich, F.; Hauert, R.; Stewart, J. A.; Curulla Ferré, D.; Pérez-Ramírez, J. Role of Zirconia in Indium Oxide-Catalyzed CO₂ Hydrogenation to Methanol. *ACS Catal.* **2020**, *10* (2), 1133–1145.
- (137) Martin, O.; Martin, A. J.; Mondelli, C.; Mitchell, S.; Segawa, T. F.; Hauert, R.; Drouilly, C.; Curulla-Ferre, D.; Perez-Ramirez, J. Indium Oxide as a Superior Catalyst for Methanol Synthesis by CO₂ Hydrogenation. *Angew. Chem., Int. Ed. Engl.* **2016**, *55* (21), *6261–5*.
- (138) Wang, J.; Li, G.; Li, Z.; Tang, C.; Feng, Z.; An, H.; Liu, H.; Liu, T.; Li, C. A highly selective and stable ZnO-ZrO₂ solid solution catalyst for CO₂ hydrogenation to methanol. *Sci. Adv.* **2017**, 3, 1701290.
- (139) Chou, C.-Y.; Lobo, R. F. Direct conversion of CO₂ into methanol over promoted indium oxide-based catalysts. *Appl. Catal. A-Gen.* **2019**, 583, 117144.
- (140) Tsoukalou, A.; Abdala, P. M.; Stoian, D.; Huang, X.; Willinger, M. G.; Fedorov, A.; Muller, C. R. Structural Evolution and Dynamics of an In₂O₃ Catalyst for CO₂ Hydrogenation to Methanol: An Operando XAS-XRD and In Situ TEM Study. *J. Am. Chem. Soc.* **2019**, 141 (34), 13497–13505.
- (141) Sun, K.; Fan, Z.; Ye, J.; Yan, J.; Ge, Q.; Li, Y.; He, W.; Yang, W.; Liu, C.-j. Hydrogenation of CO_2 to methanol over In_2O_3 catalyst. *J. CO2 Util.* **2015**, *12*, 1–6.
- (142) Ye, J.; Liu, C.; Mei, D.; Ge, Q. Active Oxygen Vacancy Site for Methanol Synthesis from CO₂ Hydrogenation on In₂O₃(110): A DFT Study. ACS Catal. **2013**, 3 (6), 1296–1306.
- (143) Frei, M. S.; Mondelli, C.; Garcia-Muelas, R.; Kley, K. S.; Puertolas, B.; Lopez, N.; Safonova, O. V.; Stewart, J. A.; Curulla Ferre, D.; Perez-Ramirez, J. Atomic-scale engineering of indium oxide promotion by palladium for methanol production via CO₂ hydrogenation. *Nat. Commun.* **2019**, *10* (1), 3377.
- (144) Jiang, X.; Nie, X.; Gong, Y.; Moran, C. M.; Wang, J.; Zhu, J.; Chang, H.; Guo, X.; Walton, K. S.; Song, C. A combined experimental and DFT study of H₂O effect on In₂O₃/ZrO₂ catalyst for CO₂ hydrogenation to methanol. *J. Catal.* **2020**, *383*, 283–296.
- (145) Campbell, C. T.; Daube, K. A.; White, J. M. Cu/ZnO (0001) and ZnO_x/Cu (111): model catalysts for methanol synthesis. *Surf. Sci.* 1987, 182 (3), 458–476.

- (146) Yang, Y.; Evans, J.; Rodriguez, J. A.; White, M. G.; Liu, P. Fundamental studies of methanol synthesis from CO₂ hydrogenation on Cu(111), Cu clusters, and Cu/ZnO(0001). *Phys. Chem. Chem. Phys.* **2010**, 12 (33), 9909–17.
- (147) Kattel, S.; Ramirez, P. J.; Chen, J. G.; Rodriguez, J. A.; Liu, P. Active sites for CO₂ hydrogenation to methanol on Cu/ZnO catalysts. *Science* **2017**, 355 (6331), 1296–1299.
- (148) Wen, J.; Huang, C.; Sun, Y.; Liang, L.; Zhang, Y.; Zhang, Y.; Fu, M.; Wu, J.; Chen, L.; Ye, D. The Study of Reverse Water Gas Shift Reaction Activity over Different Interfaces: The Design of Cu-Plate ZnO Model Catalysts. *Catalysts* **2020**, *10* (5), 533.
- (149) Sun, Y.; Huang, C.; Chen, L.; Zhang, Y.; Fu, M.; Wu, J.; Ye, D. Active site structure study of Cu/Plate ZnO model catalysts for CO_2 hydrogenation to methanol under the real reaction conditions. *J. CO2 Util.* **2020**, *37*, 55–64.
- (150) Le Valant, A.; Comminges, C.; Tisseraud, C.; Canaff, C.; Pinard, L.; Pouilloux, Y. The Cu-ZnO synergy in methanol synthesis from CO₂, Part 1: Origin of active site explained by experimental studies and a sphere contact quantification model on Cu + ZnO mechanical mixtures. *J. Catal.* **2015**, 324, 41–49.
- (151) Eren, B.; Weatherup, R. S.; Liakakos, N.; Somorjai, G. A.; Salmeron, M. Dissociative Carbon Dioxide Adsorption and Morphological Changes on Cu(100) and Cu(111) at Ambient Pressures. J. Am. Chem. Soc. 2016, 138 (26), 8207–11.
- (152) Ouyang, B.; Tan, W.; Liu, B. Morphology effect of nanostructure ceria on the Cu/CeO₂ catalysts for synthesis of methanol from CO₂ hydrogenation. *Catal. Commun.* **2017**, *95*, 36–39.
- (153) Pagán-Torres, Y. J.; Lu, J.; Nikolla, E.; Alba-Rubio, A. C.Well-Defined Nanostructures for Catalysis by Atomic Layer Deposition. In *Morphological, Compositional, and Shape Control of Materials for Catalysis*; Fornasiero, P., Cargnello, M., Eds.; Elsevier: 2017; pp 643–676.
- (154) Héroguel, F.; Rozmyslowicz, B.; Luterbacher, J. S. Improving Heterogeneous Catalyst Stability for Liquid-phase Biomass Conversion and Reforming. *Chimia (Aarau)* **2015**, *69* (10), 582–91.
- (155) Johnson, R. W.; Hultqvist, A.; Bent, S. F. A brief review of atomic layer deposition: from fundamentals to applications. *Mater. Today* **2014**, *17* (5), 236–246.
- (156) Héroguel, F.; Le Monnier, B. P.; Brown, K. S.; Siu, J. C.; Luterbacher, J. S. Catalyst stabilization by stoichiometrically limited layer-by-layer overcoating in liquid media. *Appl. Catal. B-Environ.* **2017**, 218, 643–649.
- (157) Le Monnier, B. P.; Wells, F.; Talebkeikhah, F.; Luterbacher, J. S. Atomic Layer Deposition on Dispersed Materials in Liquid Phase by Stoichiometrically Limited Injections. *Adv. Mater.* **2019**, *31* (52), No. e1904276.
- (158) Liu, C.; Nauert, S. L.; Alsina, M. A.; Wang, D.; Grant, A.; He, K.; Weitz, E.; Nolan, M.; Gray, K. A.; Notestein, J. M. Role of surface reconstruction on Cu/TiO₂ nanotubes for CO₂ conversion. *Appl. Catal. B-Environ.* **2019**, 255, 117754.
- (159) Zhang, X.; Han, S.; Zhu, B.; Zhang, G.; Li, X.; Gao, Y.; Wu, Z.; Yang, B.; Liu, Y.; Baaziz, W.; Ersen, O.; Gu, M.; Miller, J. T.; Liu, W. Reversible loss of core-shell structure for Ni-Au bimetallic nanoparticles during CO₂ hydrogenation. *Nat. Catal.* **2020**, 3 (4), 411–417
- (160) Matsubu, J. C.; Zhang, S.; DeRita, L.; Marinkovic, N. S.; Chen, J. G.; Graham, G. W.; Pan, X.; Christopher, P. Adsorbate-mediated strong metal-support interactions in oxide-supported Rh catalysts. *Nat. Chem.* **2017**, *9* (2), 120–127.
- (161) Chandler, B. D. Strong metal-support interactions: An extra layer of complexity. *Nat. Chem.* **2017**, *9* (2), 108–109.
- (162) Zhang, J.; Wang, H.; Wang, L.; Ali, S.; Wang, C.; Wang, L.; Meng, X.; Li, B.; Su, D. S.; Xiao, F. S. Wet-Chemistry Strong Metal-Support Interactions in Titania-Supported Au Catalysts. *J. Am. Chem. Soc.* **2019**, *141* (7), 2975–2983.